EBioMedicine 45 (2019) 39–57

Contents lists available at ScienceDirect

EBioMedicine

journal homepage: www.ebiomedicine.com

EBioMedicine
Published by THE LANCET

Combinatorial targeting of cancer bone metastasis using mRNA engineered stem cells

Aude I. Segaliny [a,b,c,d,e,f], Jason L. Cheng [a,b,c,d,e,f], Henry P. Farhoodi [a,b,c,d,e,f], Michael Toledano [a,b,c,d,e,f], Chih Chun Yu [a,b,c,d,e,f], Beatrice Tierra [i], Leanne Hildebrand [a,b,c,d,e,f], Linan Liu [a,b,c,d,e,f], Michael J. Liao [a,b,c,d,e,f], Jaedu Cho [g], Dongxu Liu [h], Lizhi Sun [h], Gultekin Gulsen [g], Min-Ying Su [g], Robert L. Sah [i], Weian Zhao [a,b,c,d,e,f,*]

[a] Sue and Bill Gross Stem Cell Research Center, University of California, Irvine, Irvine, CA 92697, USA
[b] Department of Pharmaceutical Sciences, University of California, Irvine, Irvine, CA 92697, USA
[c] Chao Family Comprehensive Cancer Center, University of California, Irvine, Irvine, CA 92697, USA
[d] Edwards Life Sciences Center for Advanced Cardiovascular Technology, University of California, Irvine, Irvine, CA 92697, USA
[e] Department of Biomedical Engineering, University of California, Irvine, Irvine, CA 92697, USA
[f] Department of Biological Chemistry, University of California, Irvine, Irvine, CA 92697, USA
[g] Department of Radiological Sciences, University of California, Irvine, Irvine, CA 92697, USA
[h] Department of Civil and Environmental Engineering, University of California, Irvine, Irvine, CA 92697, USA
[i] Department of Bioengineering, University of California, San Diego, San Diego, CA 92093, USA

ARTICLE INFO

Article history:
Received 17 June 2019
Received in revised form 22 June 2019
Accepted 24 June 2019
Available online 4 July 2019

Keywords:
Bone metastases
Cell therapy
Mesenchymal stem cell
mRNA engineering
Combination therapy

ABSTRACT

Background: Bone metastases are common and devastating to cancer patients. Existing treatments do not specifically target the disease sites and are therefore ineffective and systemically toxic. Here we present a new strategy to treat bone metastasis by targeting both the cancer cells ("the seed"), and their surrounding niche ("the soil"), using stem cells engineered to home to the bone metastatic niche and to maximise local delivery of multiple therapeutic factors.

Methods: We used mesenchymal stem cells engineered using mRNA to simultaneously express P-selectin glycoprotein ligand-1 (PSGL-1)/Sialyl-Lewis X (SLEX) (homing factors), and modified versions of cytosine deaminase (CD) and osteoprotegerin (OPG) (therapeutic factors) to target and treat breast cancer bone metastases in two mouse models, a xenograft intratibial model and a syngeneic model of spontaneous bone metastasis.

Findings: We first confirmed that MSC engineered using mRNA produced functional proteins (PSGL-1/SLEX, CD and OPG) using various *in vitro* assays. We then demonstrated that mRNA-engineered MSC exhibit enhanced homing to the bone metastatic niche likely through interactions between PSGL-1/SLEX and P-selectin expressed on tumour vasculature. In both the xenograft intratibial model and syngeneic model of spontaneous bone metastasis, engineered MSC can effectively kill tumour cells and preserve bone integrity. The engineered MSC also exhibited minimal toxicity *in vivo*, compared to its non-targeted chemotherapy counterpart (5-fluorouracil).

Interpretation: Our combinatorial targeting of both the cancer cells and the niche represents a simple, safe and effective way to treat metastatic bone diseases, otherwise difficult to manage with existing strategies. It can also be applied to other cell types (*e.g.*, T cells) and cargos (*e.g.*, genome editing components) to treat a broad range of cancer and other complex diseases.

Fund: National Institutes of Health, National Cancer Institute of the National Institutes of Health, Department of Defense, California Institute of Regenerative Medicine, National Science Foundation, Baylx Inc., and Fondation ARC pour la recherche sur le cancer.

1. Introduction

Bone metastasis is one of the most common complications in many cancers, and is present in over 350,000 people who die each year in the United States [1]. Bone metastases are incurable, largely untreatable, and have devastating effects on quality of life. They occur in up to 70% of patients with advanced breast cancer, and are associated with a

* Corresponding author at: Sue & Bill Gross Hall CIRM Institute, 845 Health Sciences Road, Suite 3027, Irvine, CA 92697, USA.
E-mail address: weianz@uci.edu (W. Zhao).

https://doi.org/10.1016/j.ebiom.2019.06.047

Research in context

Evidence before this study

There are no cures for breast cancer bone metastases. We first surveyed the state-of-the-art for treatments currently used to treat bone metastases, and more specifically in breast cancer. We also looked for preclinical research, including targeted therapy such as nanoparticles or new chemistries (bisphosphonates, *etc.*). The search was done periodically using scientific database including PubMed, Web of Science and Google Scholar as well as for clinical trials on https://clinicaltrials.gov/. Importantly, existing approaches do not sufficiently target both the cancer and the tumour niche. Mesenchymal stem cells (MSC) appeared to be ideal candidates to deliver treatments to bone metastases due to their ability to home to the bone marrow and tumour sites, as shown by multiple reports including clinical studies. We therefore sought to engineer MSC using our previously established mRNA engineering strategy to develop a targeted, combinatorial platform to block the vicious cycle between tumour growth and bone destruction.

Added value of this study

Using two animal models of breast cancer bone metastases: one immunocompromised intratibial model (human breast cancer) and one syngeneic model of spontaneous bone metastases (murine breast cancer), we demonstrated for the first time that mRNA engineered MSC could be used as a powerful platform to target and treat bone metastases in breast cancer following systemic infusion, by efficiently homing to the bone metastatic niche and co-delivering therapeutics that induce tumour killing and inhibit tumour-induced bone resorption. In addition, this targeted treatment approach exhibited minimal unwanted toxicity.

Implications of all the available evidence

Our study suggests targeted, combined therapies targeting both cancer and the tumour niche can potentially be safer and more effective to treat bone metastases than monotherapies and non-targeted treatments (*e.g.* chemotherapies). This platform technology is modular and could be applied to other types of tumours or diseases that require delivery of multiple cargos. Moving towards clinical studies, future work should systematically study the dosage, number, frequency and schedules of treatments, potentially together with patient stratification based on disease stages, in order to obtain optimal therapeutic outcomes especially in the long-term. Furthermore, an optimal therapeutic schedule should be identified (sequential injections, repeated treatments and mixing of MSC engineered differently).

median-survival of 19–25 months, along with severe morbidities including intractable pain, pathological fractures, spinal cord compression, and hypercalcemia [2]. Breast cancer cells alter the bone microenvironment and produce factors to promote osteoclastogenesis. In turn, bone resorption by osteoclasts releases growth factors, which stimulate tumour progression [3]. The reciprocal interaction between breast cancer cells and the bone microenvironment, called the "vicious cycle," accelerates tumour growth and bone destruction. An effective therapy to treat bone metastasis, therefore, would require efficient targeting of both the cancer cells and their microenvironment. Such a treatment has been lacking. In fact, despite major progress in cancer therapies, the 5-year relative survival rate for metastatic breast cancer has barely improved over the past 20 years, remaining around 20% [2,4]. Common treatments including surgery, chemotherapy, radiation therapy, and endocrine therapy are only palliative and are often associated with significant systemic toxicity [5]. Standard of care drugs targeting bone resorption, including bisphosphonates and Denosumab (antibody targeting the receptor activator of NF-κB ligand, RANKL), which act by inhibiting osteoclastogenesis through different mechanisms, are controversial in their anti-tumour mechanisms [6,7]. Most importantly, these therapies, alone or in combination, are ineffective in targeting both tumour growth and osteolysis, often leading to relapse, new metastasis, drug resistance, and notably, high systemic toxicity [8]. In addition, targeted drug delivery systems for bone metastasis, especially those using nanoparticles, are still in their infancy [9–13], and typically suffer from rapid clearance, poor targeting efficiency, and inability to penetrate to the centre of large and poorly vascularised metastatic tumours [14].

Here we exploit a stem cell based approach for targeted delivery of a combination of therapeutics, which interrogates both the cancer and its niche. Stem cells, including mesenchymal stem (or stromal) cells (MSC), act as potent, autonomous, and adaptive agents [15,16], and have recently been tested as vehicles for drug delivery in cancer [17–22], including in clinical trials [23]. Specifically, using a facile mRNA-engineering approach, we programmed mesenchymal stem cells with machinery to enable a) specific and efficient bone metastasis homing through engineered P-selectin glycoprotein ligand-1 (PSGL-1) and Sialyl-Lewis X (SLEX), which target highly expressed selectins in vessels surrounding the tumour [24–26], b) local cancer killing through the cytosine deaminase (CD)/pro-drug 5-Fluorocytosine (5-FC) system [27], and c) osteolysis inhibition within the tumour niche through expression of modified osteoprotegerin (OPG) [28], a natural decoy receptor for RANKL, a key mediator in tumour-induced osteoclastogenesis (Fig. 1). Previous studies targeting bone tumours through a cell-based therapy approach used genetically modified cells to only deliver a single therapeutic molecule [29–31]. Engineering cells with mRNA-based protein expression is advantageous for targeting bone metastasis due to its simplicity, safety (no genetic engineering), transient and rapid protein translation after transfection, and ability to express multiple factors simultaneously for combinatorial treatment [32–34]. In this report, using a xenograft intratibial model and a syngeneic model of spontaneous bone metastasis, we demonstrated that MSC engineered to simultaneously express PSGL-1/SLEX, CD, and OPG exhibit enhanced homing to the bone metastatic niche where they effectively kill tumour cells and preserve bone integrity with minimal toxicity.

2. Methods

2.1. Ethics statement

All studies were done in accordance with National Institutes of Health guidelines for care and use of animals under approval of the Institutional Animal Care and Use Committees of the University of California, Irvine (IACUC protocol #AUP-18-134).

2.2. Reagents

Minimum Essential Medium α, Roswell Park Memorial Institute (RPMI) 1640 Medium, Dulbecco's Modified Eagle Medium, Leibowitz' L-15 Medium, EGM-2 Endothelial Cell Growth Medium, M-199 Medium, Endothelial Cell Growth Suspension (ECGS), Penicillin/streptomycin solution, 2% gelatin solution, Opti-MEM Reduced Serum Medium, RNAiMAX Lipofectamine, 10× Tris-buffered saline (TBS), Scott's Bluing Solution, Fisherfinest Histoplast paraffin, MX35 Ultra low-profile cryotome blades, polylysine slides, HPLC grade ethyl acetate, acetonitrile, ACS grade glacial acetic acid, 2-propanol, recombinant human TNF-α, recombinant human OPG, recombinant murine RANKL, Vybrant™ DiD lipophilic dye, CellTrace™ Calcein Green dye and 7-AAD viability assay dye were purchased from Fisher Scientific. 4% paraformaldehyde (PFA) solution was purchased from Santa Cruz Biotechnology. Recombinant human TRAIL was obtained from Peprotech. Fetal bovine serum (FBS), sterile phosphate-buffered saline (PBS), ACK

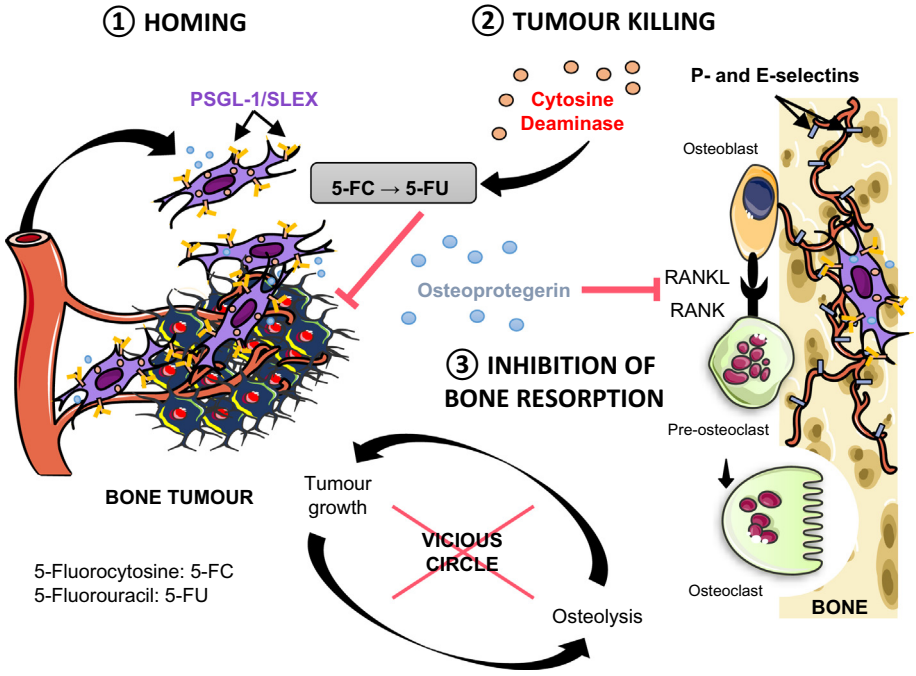

Fig. 1. Combinatorial targeting of cancer bone metastasis using mRNA engineered mesenchymal stem cells. Proposed strategy for bone metastasis treatment by targeted delivery of multiple factors using mRNA-engineered mesenchymal stem cell (MSC) equipped with functions for a) specific and efficient bone metastases homing through P-selectin glycoprotein ligand-1 (PSGL-1) and Sialyl-Lewis X (SLEX), b) local cancer killing through cytosine deaminase (CD)/pro-drug 5-Fluorocytosine, and c) osteolysis inhibition within the tumour niche through a modified version of RANKL decoy receptor, osteoprotegerin (OPG).

lysis Buffer, Tissue-Tek Optimal Cutting Temperature (OCT) embedding medium and Superfrost Plus slides were purchased from VWR. Puromycin powder, crystalline bovine serum albumin (BSA), Tween 20, Triton X-100, as well as donkey and goat normal sera, Harris' Haematoxylin, Eosin Y, 2-methylbutane, 10% Formalin solution, sucrose, EDTA, 5-Fluorouracil (5-FU), and 5-Fluorocytosine (5-FC) were purchased from MilliporeSigma. Isoflurane was purchased from Piramal Healthcare. Ketamine, xylazine, and buprenorphine were purchased from Western Medical Supply. D-luciferase was purchased from Perkin Elmer. Histo-Clear II was used as a xylene substitute for dehydration of tissue samples and was purchased from National Diagnostics. Water was purified using the Millipore Milli-Q system.

2.3. Cell culture

MDA-MB-231 human ductal adenocarcinoma cells, 4T1 murine breast cancer, RAW264.7 macrophages, and HL-60 promyeloblasts were purchased from American Type Culture Collection, Inc. (ATCC) and respectively cultured in Leibovitz' L-15 medium, RPMI medium, Dulbecco's Modified Eagle Medium and RPMI medium supplemented with 10% FBS. MDA-MB-231 and 4T1 cells were transduced to express both firefly luciferase enzyme and RFP (LucF/RFP) using CMV-Luc3-2A-RFP (Puro) lentiviral particles (GenTarget, San Diego, CA, USA) per the manufacturer's protocol. Briefly, 1×10^4 cells were seeded in a 24-well plate and infected with a multiplicity of infection of 10 particles/cell. 72 hours post-transduction, media was replaced with fresh media containing 20 μg/mL puromycin for selection. 5 μg/mL puromycin was used for routine culture to maintain transduction. LucF/RFP 4T1 CLL1 cells were *in vivo* selected from a mouse femur metastasis, which arose from a mammary fat pad injection of LucF/RFP 4T1 cells. 4T1 CLL1 were cultured similarly to parental 4T1 cells. Human mesenchymal stem cells (MSC), obtained under principles of informed consent from the bone marrow of a healthy donor (#8011L), were purchased from Texas A&M Institute for Regenerative Medicine (Bryan, TX, USA), a NIH-funded non-profit organisation for MSC isolation, characterisation and distribution. These cells were fully characterised per established guidelines [35,36]: MSC were tested for presence of viruses (HIV, hepatitis, *etc.*), characterised by their ability to differentiate into bone and fat, and by their negative expression for CD45, CD19, CD34, CD11b, CD79a, HLA-II:DR DQ DP, CD14 and positive expression for CD90, CD105, CD73a. MSC were cultured in Minimum Essential Medium-α enriched with 15% FBS, 2% L-glutamine, and 1% penicillin-streptomycin solution. To further characterise if engineering affects MSC function, we performed additional osteogenic and adipogenic differentiations of our engineered MSC (Supplementary Fig. 1). Specifically, PSGL-1/SLEX/CD/OPG MSC were seeded onto 24-well tissue culture plates at a density of 6×10^4 cells/well and cultured for 2–3 weeks. The media was made from Osteogenesis or Adipogenesis Differentiation Kits (EMD Millipore) and changed according to the manufacturer's instructions. At the end-point, cells were fixed and stained with Alizarin Red-S or Oil-Red-O, according to the manufacturer's instructions. Human umbilical vein endothelial cells (HUVEC) were kindly provided by Dr. Hughes (Department of Cellular and Molecular Biosciences, University of California, Irvine) and cultured in M-199 medium supplemented with 10% FBS, 2% L-glutamine, 1% penicillin-streptomycin solution, and 50 μg/mL ECGS. MDA-MB231 LucF/RFP were cultured without CO_2.

2.4. mRNA synthesis and cell engineering

mRNA were synthesised by TriLink BioTechnologies (San Diego, CA, USA) as previously described using *in vitro* transcription [32, 34]. mRNA were capped and modified with a polyadenylated tail along with pseudouridine and 5-methylcytidine bases to decrease immunogenicity, enhance translation, and enhance stability. DNA coding sequences used for the mRNA synthesis are specified in Supplementary Table 1. P2 MSC were transfected with Lipofectamine RNAiMAX in Opti-MEM reduced serum medium at 80% confluency using 1 μg mRNA per 10 cm^2 of surface area.

2.5. Cytometry

A minimum of 150,000 cells was used for all membrane staining. Cells were washed and stained in 1% BSA in PBS on ice. 7-AAD was used as a viability dye at a concentration of 5 μg/mL and antibodies

were used at 4 μg/mL (Supplementary Table 1). For apoptosis staining, 5 μL of Annexin V-FITC was added to 100 μL of cells re-suspended at 1 × 10^6 cells/mL in binding buffer, following the manufacturer's recommendations. A minimum of 10,000 events were collected in the gates of interest. Unstained and single stained cells were used to generate the compensation matrix. An example of the gating strategy used for the analysis is shown in Supplementary Fig. 2. Flow cytometry was performed on an Accuri C6 flow cytometer and an LSR II flow cytometer (BD Biosciences, San Jose, CA, USA). Data were analysed using FlowJo version 10.1 software.

2.6. Immunofluorescence

For immunohistochemistry and immunofluorescence, 8 μm sections were rehydrated using TBS. When necessary, tissue was permeabilised for 15 min with Tween 20 or Triton X-100. Blocking was done for 30 min using 5% normal serum from the appropriate species, diluted in a 1% BSA TBS solution. Primary antibodies were added at designated dilutions in blocking buffer (Supplementary Table 1) and incubated at 4 °C overnight. Primary antibody binding was detected using appropriate secondary antibodies incubated at room temperature for 60 min, and mounting was done using Fluoromount G containing DAPI (Southern Biotech) and 0.17 mm glass coverslips.

For the quantification of P-selectin expression, we selected 200 μm by 200 μm areas within the tibia containing MSC, and the average P-selectin signal was measured by dividing total photon counts emitted in Cy5 channel per surface area and subtracting the background signal. To evaluate how P-selectin expression varied depending on the distance from the tumour, we randomly selected large longitudinal leg sections containing both tumour and at least 900 μm of marrow. We used NIS-Elements AR Analysis 4.50.00 64-bit grid utility (Nikon) to automatically generate a grid with 100 μm by 100 μm squares (ROIs) covering the whole marrow section. All ROIs not covering marrow vasculature were excluded. Automated measurement calculated the mean fluorescent signal for each ROI, and background was subtracted for each. The ROIs were assigned a distance from the tumour per 100 μm by 100 μm area, and P-selectin signal, and average signal was calculated per distance area from the tumour.

2.7. Western blotting

Cell lysates were prepared using an SDS-based buffer, and subsequent protein concentration was determined using a standard bicinchoninic acid (BCA) assay. 40 μg of proteins were separated using SDS-PAGE and transferred to Immun-Blot PVDF Membrane (Biorad, Hercules, CA, USA). After blocking in a 5% milk TBS-Tween solution, the membrane was blotted overnight at 4 °C with primary antibodies directed against cytosine deaminase, Fc specific human IgG, and GAPDH before being probed with secondary antibodies conjugated to horseradish peroxidase for 1 h at RT (Supplementary Table 1). After incubation with ECL substrate (Fisher Scientific), luminescence was detected using a ChemiDoc XRS+ (Bio-rad) and quantified using Image Lab 3.0.1 Beta 2 (Bio-rad).

2.8. ELISA

OPG concentration was measured in culture supernatants of MSC using a human osteoprotegerin/TNFRSF11B DuoSet ELISA (R&D Systems) according to the manufacturer's recommendations. Each supernatant was assessed undiluted, diluted 1:10, and diluted 1:50 to be quantified in the linear range, and dosed in duplicates. As a control, 1 ng/mL of recombinant human OPG was included in the assays.

2.9. Flow chamber assay

5 × 10^5 P-2 HUVEC were seeded onto 35 × 10 mm Petri dishes (Corning) coated with 1% gelatin (Sigma) and incubated for one day to reach confluence. HUVEC were stimulated using 50 ng/mL human TNF-α 6 h prior to the assay to induce selectin expression. A flow chamber assay was performed using a PicoPlus syringe pump (Harvard Apparatus, Holliston, MA, USA) set at four different flow rates (4.42 μL/min to create 1 dyn/cm^2 shear force, 8.84 μL/min for 2 dyn/cm^2, 17.68 μL/min for 5 dyn/cm^2, and 35.36 μL/min for 10 dyn/cm^2), and a vacuum pump (Welch, Mt. Prospect, IL, USA) collecting post-chamber efflux. Briefly, 1 × 10^6 cells/mL of each cell type to be assayed were stained with 2.5 μM CellTrace™ Calcein Green dye for better quantification using fluorescence, suspended in fresh EGM-2, and loaded in a 1 mL syringe attached to the syringe pump. A flow chamber gasket (GlycoTech, Gaithersburg, MD, USA) was attached to the top of the HUVEC-seeded petri dish, a Silastic™ (GlycoTech) fluid line was fixed to the tip of the syringe and connected to the inflow port of the flow chamber gasket, and a drain line was run from the outflow port of the gasket to the waste chamber of the vacuum pump. 300 μL of cell suspension was injected across the HUVEC layer for each run.

2.10. MDA-MB-231/MSC co-killing assays

On day 0, MSC were engineered using mRNA transfection. On day 1, MDA-MB231 LucF/RFP cells were respectively plated in a 96-well plate at 1.5 × 10^4 cells per well and in a 24-well plate at 1 × 10^5 cells per well, to reach 90% confluency on day 2. On day 3, depending on the assay conditions, 5-FC or 5-FU was added, and different ratios of MSC were plated on top of cancer cells in MSC culture media. On day 9, the 24-well plate was imaged using brightfield and fluorescence to visualise the co-culture and MDA-MB-231 expressing RFP. The 96-well plate was incubated with AlamarBlue™ (Fisher Scientific) at a 1:10 dilution in 100 μL fresh culture medium to measure the viability of the co-culture. After 5 to 6 h, the absorbance was measured at a wavelength of 570 nm (the peak absorbance for the reduced form) and 600 nm (peak absorbance for the oxidised form) using a plate reader (Synergy HT, Biotek, Winooski, VT, USA). Briefly, the metabolic growth (and thereby the viability) of the cells was determined by subtracting the absorbance of the oxidised form from that of the reduced form. Data were normalised to the control (untreated cells).

2.11. TRAIL-OPG assay

Concentrated media enriched for osteoprotegerin was generated by centrifuging 15 mL of conditioned media from MSC (day 3 post-engineering) using a 30 kDa Amicon Ultra-15 centrifugal filter unit (EMD Millipore, Temecula, CA, U.S.A.) at 4000*g* for 15 min. MDA-MB-231 cells were plated in a 96-well plate at a density of 1.5 × 10^4 cells/well and treated with recombinant human TRAIL in addition to rhOPG or concentrated MSC supernatant containing an equivalent concentration of OPG (as determined by ELISA).

2.12. Osteoclastic differentiation

Murine macrophages RAW264.7 cells were seeded at 1 × 10^3 cells per well in a 96-well plate and treated with 100 ng/mL murine RANKL in addition to human OPG or concentrated supernatant of MSC (from day 3 post-engineering). Medium was changed every other day. Each condition was performed in triplicate for each independent experiment. At day 6, cells were washed and fixed with 4% PFA and thenTRAP stained using the Acid Phosphatase, Leukocyte (TRAP) Kit (MilliporeSigma) per manufacturer's instructions, with a 1:100 Harris' haematoxylin dilution in water for counterstaining. The entire wells were imaged under a light microscope and multinucleated TRAP-positive osteoclasts with >3 nuclei were counted.

2.13. LC-MS/MS for 5-FU quantification

2.13.1. Generation of conditioned media

MSC were seeded to a 24-well plate at 0.1×10^5, 0.5×10^5 and 1.0×10^5 cells per well in the presence of 400 μg/mL 5-FC. At different time-points (1 to 6 days), media was collected, centrifuged to remove floating cells and debris, and frozen at −80 °C until chemical extraction.

2.13.2. Compound extraction

To determine the extraction yield, culture medium was spiked with known concentrations of 5-FU (50 and 100 μg/mL). 250 μL of conditioned media sample was processed using 1.75 mL extraction buffer (1:1 ethyl acetate/2-propanol). After incubation and agitation, tubes were centrifuged at 3000*g* for 10 min, and the organic layers were collected. Remaining proteins were precipitated from the organic layers by adding 100 μL saturated ammonium sulphate solution. After centrifugation, the organic phases were transferred to new centrifuge tubes and the solvent was evaporated in a Savant DNA120 SpeedVac Concentrator (ThermoScientific, Waltham, MA, USA). Extracted compounds were then resuspended for LC-MS/MS in analysis buffer (Milli-Q water containing 2% acetonitrile and 0.2% acetic acid, similar to the mobile phase A used for the UPLC).

2.13.3. LC-MS/MS analysis

10 μL of extract was injected into an Acquity UPLC system (Waters Corporation, Milford, MA, USA) and separated with an Acquity UPLC-BEH C18 1.7 μm, 2.1 × 50 mm analytical column (Waters). The autoinjector temperature was maintained at 5 °C and the column temperature at 25 °C. A gradient mobile phase elution was used, starting with 98% of solvent A (98% Milli-Q water, 2% acetonitrile and 0.2% acetic acid), and progressing in 3 min to 95% of solvent B (99.8% acetonitrile and 0.2% acetic acid) before holding in B for 60 s to elute the samples. The samples were then injected into a triple quad mass spectrometer (Waters Micromass Quattro Premier XE™ Tandem Quadrupole Mass Spectrometer, Waters) for mass analysis. Electrospray ionisation was done using the negative ion mode (ESI^-), which generates a precursor to product ion transition of m/z 128 > 85 for 5-FC and 129 > 42 for 5-FU, thus allowed discrimination of the two compounds for analysis. Cone voltage and collision cell energy were optimised using training samples: 20 V (CV) and 10 V (CE) for 5-FC, 20 V (CV) and 30 V (CE) for 5-FU. MassLynx version 4.1 software was used for data acquisition, and QuantLynx software for downstream analysis. A 7-point 5-FU standard curve was prepared in serial dilution (1/3 dilution factor) starting from 60 μg/mL down to 0 μg/mL (analysis buffer alone) in order to determine the 5-FU concentration inside the samples ($r^2 > 0.98$, quadratic fit). An example of mass spectrometry data obtained for 5-FC and 5-FU is shown in Supplementary Fig. 3.

2.14. Animal experiments

Animal subjects were first sedated in a chamber, then kept under a nosecone for the procedures, using either 2% isoflurane mixed with 2 L/min O_2, or by intraperitoneal (*i.p.*) injection of a 100 mg/kg ketamine and 10 mg/kg xylazine mixture. For all intratibial injections, animals were injected *i.p.* with 0.1 mg/kg buprenorphine for pre- and post-procedure analgesia.

To mimic established breast cancer bone metastases, 1×10^5 MDA-MB-231 LucF/RFP cells in 10 μL of sterile PBS were injected into the marrow cavity of the left tibia of 4- to 5-week-old female nude mice (strain code #194, CAnN.Cg-Foxn1^{nu}/Crl), purchased from Charles River Laboratories (Wilmington, MA, USA), using a 28Gx1/2″, 1/2 cc insulin syringe (ADW Diabetes). Note that for all studies (homing and efficacy studies) we also performed a mock PBS injection in the healthy tibia in the same animal to eliminate potential bias resulted from inflammation due to injection.

To establish a robust and spontaneous bone metastasis model [37], 1×10^4 cells of our bone metastatic clone 4T1 CLL1 LucF/RFP were injected, *via* the caudal artery (c.a), into 5-week-old female BALB/cJ mice (JAX#000651, The Jackson Laboratory, Bar Harbor, ME, USA) using 29Gx1/2″ 3/10 cc insulin syringes (ADW Diabetes). This model had a 90% incidence for bone metastases, and the majority of bone metastases were located in legs (femur/hip area) and spine, but we also found some metastases in the rib cage, the scapula and the mammary fad pad. For therapeutic treatment, MSC were injected either intratibially (1×10^5 cells in 10 μL sterile PBS) or intravenously (7×10^5–1×10^6 cells in 200 μL sterile PBS) into the lateral tail veins. 5-FC (500 mg/kg) and 5-FU (12.5 mg/kg for syngeneic model, 200 mg/kg for immunocompromised model) were injected *i.p.* in PBS. For our syngeneic model, we chose a 5-FU dose that was not overly toxic to animals but sufficient to induce anti-tumour effect based on the literature, and clinically relevant: several clinical dose recommendations for breast cancer include 375 mg/m^2 *i.v.* daily for five days every 3 weeks, which is equivalent to 12.84 mg/kg for an average American [38]. We performed a pilot study using 12.5 and 50 mg/kg of 5-FU and determined that 50 mg/kg was too toxic to animals, therefore deciding to use 12.5 mg/kg for the final study. Animals were closely monitored on an individual basis (visual examination, weight measurements).

Tumour growth inside the tibia was measured using bioluminescence. Mice were injected *i.p.* with 150 mg/kg sterile D-luciferase substrate (Perkin Elmer). After a 15 min hold time (peak of enzyme kinetics), tumour bioluminescence data were collected after 1 s and 1 min integration times using a Xenogen IVIS Lumina II multispectral imager (Caliper LifeSciences, Waltham, MA, USA). Bioluminescence data were analysed using Living Image version 4.3.1 software (Perkin Elmer, Waltham, MA, USA).

For homing experiments, DiD-labelled MSC were imaged *in vivo* and *ex vivo* using the Cy5.5 filter sets (615–665 nm excitation, 695–770 nm emission) of the Xenogen IVIS Lumina II. Animals not transplanted with DiD-labelled MSC were used as a control to subtract tissue autofluorescence and obtain true signal from labelled MSC.

For survival experiments, animals were euthanised following well-defined end-point criteria: any evidence of pain or suffering (prostration, isolation, absence of grooming, lethargy, anorexia, dehydration, *etc.*) or, in our particular model, 1) when the tumour invaded the cortical bone, which was typically equivalent to a total photon flux ≥1 $\times 10^{10}$ photons/s and was frequently accompanied by a visible limb deformity, 2) when the animal began to show signs of paraplegia, or 3) when the animal showed persistent cachexia and/or a >10% loss of body weight that was uncorrectable by supplemental nutrition and fluids.

The progression of paralysis in mice was assessed on a three point scale. A score of zero indicated free mouse movement with no obvious signs of paralysis. A score of one indicated the presence of retracted limbs, hunched posture, and visible trouble moving around. A score of one and a half indicated greatly restricted movement of hind limbs, which neared paralysis. A score of two indicated total paralysis of the hind limbs.

2.15. Bone marrow isolation

Mouse femurs and tibias were harvested immediately after sacrifice, and bones were thoroughly cleaned of all muscle tissue. Epiphyses were cut to expose the bone marrow cavity and bones were centrifuged in a perforated tube at 12,000*g* for 30 s to isolate the bone marrow in a collection tube. Extracted marrow was washed in PBS then incubated in ACK lysis buffer at 37 °C for 3 min to lyse erythrocytes. After quenching with PBS, the bone marrow suspension was resuspended in PBS-BSA 1% at the desired concentration for subsequent flow-cytometry analysis.

2.16. Alu qPCR analysis for MSC homing

Whole legs were harvested after euthanasia, stripped down to a thin layer of muscle surrounding the bones (muscle prevents loss of fragilised bones fragments), and flash frozen in slurry of 70% ethanol and dry ice. Surgical tools were cleaned in between each leg to prevent cross contaminations. Tissues were thawed and immediately homogenised with mechanical force using metal bead agitation at 4 °C (Next Advance Bullet Blender® Storm with Navy 5 mL Lysis Kit). DNA extraction was performed on 25 mg of homogenised tissues (1/28th of the initial lysate) using chemical lysis and silica spin column purification (Qiagen DNeasy® Blood and Tissue Kit).

To quantify human MSC numbers in each mouse leg, an Alu qPCR assay was performed on 50 ng of extracted DNA using PowerUp™ SYBR™ Green Master Mix (Applied Biosystems, Dun Laoghaire, Ireland), optimised primer sets for the human Alu transposable element (FWD: CACCTGTAATCCCAGCACTTT and REV: CCCAGGCTGGAGTGCAGT) [39], and the mouse GAPDH gene as an endogenous control (FWD: TGGCCTTCCGTGTTCCTAC and REV: GAGTTGCTGTTGAAGTCGCA) [40]. A QuantStudio™ 6 Flex Real-Time PCR System was used to run the qPCR, and data were analysed using QuantStudio™ 6 and 7 Flex Real-Time PCR System Software (Applied Biosystems, Dun Laoghaire, Ireland). A comparative CT value (ΔCT) for human MSC in each tissue was derived by subtracting the mean of triplicate mGAPDH CT values from the mean of triplicate hAlu CT values [41].

A standard curve was established by injecting known quantities of MSC into the tibias of BALB/cJ mice following 6 fold serial dilutions of the cell suspension (100, 600, 3600, 21,600 and 130,000 MSC), followed by tissue homogenisation/DNA extraction/qPCR (as described above). The logarithm of the number of MSC injected was plotted *versus* the ΔCT, and a linear regression was done to generate a standard curve slope equation. Cell numbers in each sample leg were calculated by the standard curve equation from the obtained ΔCT value. The limit of detection was determined by subtracting 2 from the negative control (PBS injection only in the mouse tibia) ΔCT value [42].

2.17. Bone micro-computed analysis and bone damage scoring

Mouse tibias were fixed in 4% PFA for 48 h immediately after dissection. After tissue fixation, samples were transferred to a radiotransparent container in sterile PBS. For our initial study, 3D X-Ray imaging was performed using VersaXRM™ 410 (Xradia, Pleasanton, CA, USA) with 14 μm voxel size. 3D volumes for whole tibias and trabecular bone were reconstructed into DICOM files for segmentation using ScanIP software (Ver. 7.0, Simpleware Ltd). ROIs were defined as the following: 1) epiphysis of the tibia down to the fibula insertion point for the whole tibia reconstruction, and 2) 100 slices (1.4 mm total) starting below the growth plate down to the diaphysis where trabeculae disappear for the trabecular bone reconstruction. Bone was segmented from the background using grayscale values, and a mask was generated from that thresholding to reconstruct the whole tibia *via* a built-in rendering function, followed by whole tibia smoothing using a "Recursive Gaussian" filter with cubic values of 2.0 cm. For trabecular reconstructions, a second ROI was generated on 2D slices after thresholding to outline the trabecular cavity and exclude the cortical bone. The morphological "Close" function was then used to fill the space in between outlines, thus generating a first mask, filling the cavity of the tibia. A "Multilevel Otsu segmentation" was applied to generate a second mask which encompassed only the background, excluding the trabecular bone. To generate a 3D trabecular bone model, a built-in rendering function was applied to a final mask resulting from the subtraction of the second mask from the first mask.

For our final studies, femur or tibia samples were imaged on a micro-Computed Tomography scanner, Skyscan 1076 (Bruker, Kontich, Belgium) at $(9\ \mu m)^3$ voxel size, 50 kVp, 200 μA and using a 0.5 mm aluminium filter. Image reconstruction was performed with NRecon software (Bruker, Kontich, Belgium) using a beam-hardening correction algorithm, at a setting of 40% and a ring artefact reduction size of 8. Samples were aligned vertically with Dataviewer software (Bruker, Kontich, Belgium). As reference points, the tips of the proximal tibial growth plate and distal femoral growth plate were noted. Then, using a custom method, an overview of each sample was visualised as 15 transverse 2D sections spaced every ~140 μm. In addition, CTvox software (Bruker, Kontich, Belgium) used with a global threshold value that selected the majority of cortical bone outline and trabecular bone to make 3D renders. Total bone volume and trabecular bone volume were analysed across 900 μm (100 slices), starting 180–360 μm from the reference point of the selected growth plate. The total bone was selected by manual contouring with elliptical cross-sections, encompassing the periosteal tissue and the marrow cavity. A global threshold was used to identify total bone and an erosion of 1–2 pixel was performed to eliminate partial volume effects. The trabecular region, inward ~100 μm from the cortex, was selected by an automated contouring routine or else by manual tracing every ~20 slices with automated interpolation. An adaptive threshold (using the mean maximum and minimum pixel intensity values of the surrounding ten pixels) was used to identify trabecular bone. The bone volume (BV) was determined using CTan (Bruker, Kontich, Belgium). For the femurs, analysis of the total BV was performed for the entirety of the femur bones.

For femur scoring, we asked 20 individuals, including 75% being unfamiliar with the research study, to blindly score each femur from the 3D reconstructions (videos and pictures). Scoring took into account the shaft damage (0: no visible damage, 1: <10% of bone missing, 2: 10–30% of bone missing and 3: extensive damage with >30% of the shaft missing) and the epiphysis damage (0: presence of both epiphysis with no damage, 1: presence of both epiphysis with little damage, 2: extensive damage/loss of one epiphysis and little to no damage on the other epiphysis, 3: extensive damage on both epiphysis, 4: loss of one epiphysis and extensive damage on the other one and 5: loss of both epiphysis).

2.18. Tissue processing

Mouse organs and limbs were respectively fixed for 24 or 48 h in 4% PFA at 4 °C. Mouse legs were then incubated in a decalcification solution (14% EDTA, 0.4% PFA (pH 7.4), in PBS) at 4 °C, on a shaker, for 14 days. Decalcification solution was changed every other day, to gently decalcify the bones. All tissues to be flash-frozen were treated in a sucrose gradient (6% then 30%) for 48 h, followed by a 6 h incubation in a 1:1 mixture of OCT and 30% sucrose solution, prior to being embedded in OCT using liquid-nitrogen-cooled isopentane. Sectioning of frozen tissue was performed on a CM1950 Ag Protect cryostat (Leica Biosystems, Wetzlar, GER) on polylysine slides using MX35 Ultra low-profile microtome blades.

Tissues destined for paraffin embedding were fixed in 10% formalin for 48 h, prior to an ethanol gradient dehydration and paraffin embedding cycle. 7 μm tissue sectioning was performed using an RM2255 microtome (Leica) with Superfrost slides.

2.19. H&E staining and TRAP staining

Haematoxylin and Eosin (H&E) staining was performed following the standard procedure, and slides were mounted using Permount (Fisher Scientific) and 0.17 mm glass coverslips. Quantifications from H&E staining were done as the following. The entire spleen sections were scanned using a 10× objective, and connective tissue was outlined and measured using NIS Elements AR Analysis area function. In order to to derive percentages, the total spleen area was divided by the sum of all connective tissue measurements. Three independent images of each animal's intestine (550 μm by 750 μm) were imaged using a 10× objective. Goblet cells were identified by absence of staining in secretory region and counted using NIS Elements AR Analysis count function per villus (only intact villi counted). Bone marrow sections were imaged

using a 20× objective, and four images were randomly selected per animal. Leukocytes were analysed on the red channel of RGB images using NIS Elements AR Analysis Spot Finder, on Dark Spot mode, "dark, clustered" profile, with a 3.5 μm expected diameter and 7.5 contrast ratio selected to differentiate between cells and morphological features. "Remove bright" was set to 90 to reject erythrocytes. Counting methodology was validated using a manual count on a small region and was found to be >99% accurate using the above settings. Total leukocyte count was divided by total enumerated region to yield a measurement of leukocytes per unit area.

TRAP staining was performed per manufacturer's protocol using the using the Acid Phosphatase, Leukocyte (TRAP) Kit. Briefly, slides were deparaffinised using histoclear and tissue rehydrated through an ethanol gradient. Tissue was then incubated in TRAP staining solution at 37 °C for 60 min, then counterstained with a 1:4 dilution of Harris' Haematoxylin in Milli-Q-water. The nuclear membranes were blued using Scott's Bluing Reagent. Slides were mounted using Aquamount medium (Fisher Scientific) under 0.17 mm cover slips. For analysis, images were cropped to select the growth plate of the tibia. A 12 mm by 12 = mm ROI was positioned to be horizontally centred relative to the growth plate, with the top edge of the ROI aligning with the highest point of the border between the proliferative and hypertrophic zones of the bone. This ROI was then duplicated to the immediate right and left of the initial counting ROI, creating a total of three counting ROI's. Osteoclasts were counted on the basis of $TRAP^+$ staining colouration, cell morphology and presence of multiple nuclei using the Cell Counter ImageJ plugin (NIH).

2.20. Microscopy

Imaging was performed using an Eclipse Ti epifluorescent microscope (Nikon, Tokyo, JPN). For brightfield imaging, the Nikon DS-Ri2 colour camera was used. For fluorescent imaging, a Lumencor Spectra X light engine was utilised to power LED light sources for excitation. Emission filters for DAPI, FITC, TRITC, Cy5, and Li-Cor 740 dyes were used, and fluorescent emissions were detected using an Andor Zyla 5.5 sCMOS camera. Confocal microscopy was performed using an Olympus FV3000RS laser-scanning confocal microscope, utilising OBIS LS/LX laser modules (Coherent, Santa Clara, CA, USA) and FV3000 Spectral Detector and High-sensitivity Spectral Detector units (Olympus, Center Valley, PA, USA). Final image processing was performed using NIS Elements Advanced Research package (Nikon) and ImageJ software (NIH).

2.21. Statistical analysis

All experiments were performed independently at least twice, and each condition within an experiment was done in duplicates or triplicates. When sample size was <30, or normal distribution and variance equality were not confirmed, non-parametric tests were used. To compare two groups, a Mann-Whitney test was performed (non-parametric *t*-test), and when comparing more than two groups a Kruskal-Wallis test was applied (non-parametric variance analysis). Both tests were followed by a multiple comparison test (adjusted *p* values for multiple comparison). For the flow-chamber assay, a two-way ANOVA test and Dunnett's multiple comparisons test was done, and each column was compared to native MSC. For the survival analysis, a log-rank (Mantel-Cox) test was performed to compare treated groups to the control group. $^*p < .05$, $^{**}p < .01$, $^{***}p < .001$ and $^{****}p < .0001$. For animal experiments, the value for each animal and the median of the group were plotted. A power analysis was done from the first animal studies performed in order to determine the minimum animal number to be used for following studies. The first study's goal was to evaluate the effect of three mRNA engineered MSC therapies (CD, OPG and CD/OPG BM-MSC) compared to PBS and Mock MSC. In our pilot data, the mean and standard deviation of the log-transferred before and after tumour growth ratio was 1.71 (1.03) in PBS group and − 0.91 (1.90) in CD/OPG group respectively. For the *ex-vivo* bone analysis, the mean (SD) of bone loss was 0.18 (0.23) for PBS group and 0.94 (0.30) for the CD/OPG group. The primary comparisons were the three-treatment groups *versus* PBS. Based on the above summary information, a sample size of 10 mice per group can achieve 81.6% power to detect the observed difference of tumour growth with an adjusted significance level at 0.0167 (=0.05/3), and a 99% power for the observed difference in bone loss. The sample size was calculated based on a two-sample two-sided *t*-test. To evaluate the efficacy of our therapies in a second animal model, we decided to compare tumour growth. The primary comparison would be the three-treatment therapies (CD, OPG and CD/OPG MSC) *v.s.* PBS group. We assumed that the effect size would be similar for this proposed study. Therefore, a sample size of 10 mice per group can achieve 84.9% power to detect the assumed difference of tumour growth with an adjusted significance level at 0.0167 (=0.05/3). A two-sample t-test was used in the sample size calculation. Bonferroni correction was applied to adjust for the three primary comparisons. For the toxicity study, the percentage of viable and necrotic cells are the two primary outcomes that reflect toxicity level and our main comparison was the three-treatment therapies (CD, OPG and CD/OPG) *v.s.* 5-FU group. In a similar study performed in immunocompromised animals, the mean difference between 5FU and CD/OPG BM-MSC triple injection was 30.3% (with SD = 16.8%) for viable cells and 40.7% (with SD = 21.9%) for necrotic cells. The proposed 10 mice per group can achieve a 90.5% power to detect the observed difference in viable cells between 5FU and CD/OPG, and 92.2% power for necrotic cells, both at significance level = 0.0167 (=0.05/3). In order to analyse our pilot study and the repeated experiment for the local injection of engineered MSC into the intratibial MDA-MB231 tumours, a linear mixed model compared the tumour growth and the bone volume among different treatment groups, with a random effect, to adjust for the potential mouse correlation within each experiment. A method of false discovery rate (FDR) was used to correct for multiple comparisons.

All graphs and statistical analysis were done using GraphPad Prism version 6.0 h for Macintosh (GraphPad Software, La Jolla, CA, USA; www.graphpad.com).

3. Results

3.1. MSC engineering using mRNA and in vitro functional validation

Modified mRNA encoding each target protein (PSGL-1, FUT-7 for post-translational SLEX modification, CD and OPG) were designed and synthesised following previous protocols [34]. We first transfected both PSGL-1 and FUT-7 mRNA into MSC, which resulted in a strong expression of fucosylated PSGL-1 at the membrane of MSC, with a typical transfection efficiency of 50–70%, as measured by flow cytometry (Supplementary Fig. 4a, b). Interestingly, positive cells tend to express both transfected factors simultaneously with few cells transfected with only a single transcript [34]. The time-course showed that expression of these markers was transient and persisted up to 6 days. Immunofluorescent staining was done 24 hours post-engineering and showed high PSGL-1 expression at the cell membrane, mainly localised in the pseudopodia (Supplementary Fig. 4c), known to be important for leukocyte rolling [43]. The functional cell rolling enabled by these engineered homing ligands was then evaluated using a standard flow chamber assay, under shear forces mimicking *in vivo* circulatory conditions. When assayed on TNF-α activated endothelial cells under 1 to 10 dyn/cm^2, Native MSC were not able to roll on the endothelium, while PSGL-1/SLEX MSC displayed a robust rolling profile comparable to that of a leukocyte model, HL-60, thus confirming the functionality of PSGL-1/SLEX modification (Fig. 2a, Supplementary Video 1). In addition, cells engineered with the four factors (PSGL-1/SLEX/CD/OPG MSC) displayed a similar rolling profile from 1 to 5 dyn/cm^2 to that of PSGL-1/SLEX MSC, suggesting that engineering cells with multiple factors has minimal effect on the functionality of the others. We next assessed the expression and function of the first therapeutic factor, OPG, which should inhibit tumour-induced bone resorption by blocking RANKL.

Note that our form of OPG is 1) truncated (no binding to glycosaminoglycans (GAGs) [44], 2) mutated (Y49R) to avoid binding to tumour necrosis factor-related apoptosis-inducing ligand (TRAIL), while preserving its binding to RANKL [29], and 3) fused to an Fc fragment of human IgG1 to increase its half-life [28] (Supplementary Table 2). As measured by ELISA, OPG accumulated over time in the culture medium of PSGL-1/SLEX/CD/OPG MSC and plateaued at approximately 70 ng/mL at day 6 (Supplementary Fig. 5a). Native MSC also secreted OPG, but at a substantially lower concentration than engineered MSC, which is common upon confluence and subsequent differentiation *in vitro*, but is unlikely to occur *in vivo* [44]. In addition, only PSGL-1/SLEX/CD/OPG MSC secreted the truncated form of OPG fused to the human IgG1 Fc fragment, as both monomers and dimers were detected in lysates of engineered MSC, but not in lysates of Native MSC when blotting for the Fc fragment (Supplementary Fig. 5b). We showed that OPG secreted by PSGL-1/SLEX/CD/OPG MSC was significantly more efficient than that of Native MSC in inhibiting osteoclastic differentiation, as osteoclast numbers decreased by 89.1% compared to the PBS control (100 ng/mL RANKL alone) (Fig. 2b). We further demonstrated that our engineered form of OPG did not block TRAIL-induced apoptosis of MDA-MB231, whereas the natural OPG protein did (Supplementary Fig. 5c), therefore mitigating its risk in preventing cancer apoptosis when used as a treatment. Finally, we characterised the expression and activity of the second therapeutic factor, cytosine deaminase fused to the UPRT (CD) [27], used for direct tumour killing. The CD/5-FC system was chosen for this study among several options for pro-drug/cytotoxic combinations[45]for different reasons. First, it is widely used in the context of cell-based delivery. It was the first suicide gene therapy protocol in the clinic (NCT02015819 and NCT0117296), and it is currently being used in clinical trials by engineered neural stem cells for treatment of glioblastoma [46]. Besides, the product 5-Fluorouracil (5-FU) is one of the standard care chemotherapy drugs for breast cancer in the clinic [47]. Finally, compared to other pro-drug/cytotoxic systems, CD/5-FC demonstrated a potent anti-tumour efficacy *in vivo* [27]. We optimised a protocol using electrospray mass spectrometry, which allows discriminating between the chemically close 5-FC and 5-FU compounds to measure the pro-drug conversion by the CD (Supplementary Fig. 3). Intracellular expression of CD was confirmed in PSGL-1/SLEX/CD/OPG MSC by both immunofluorescence and western blotting (Supplementary Fig. 6a, b). Functionally, the CD convertase was able to hydrolyse 5-FC to 5-FU, which was detected in culture supernatants with LC-MS/MS, whereas 5-FU was not found in the supernatant of Native MSC (Fig. 2c). The 5-FU concentration was dependent on the engineered cell numbers and reached up to 30 μg/mL, from 100,000 PSGL-1/SLEX/CD/OPG MSC, after 3 days of culture. Furthermore, the conversion of 5-FC into 5-FU by our mRNA-engineered MSC was shown to be as efficient as conversion by MSC constitutively expressing the CD-UPRT after lentiviral transduction [19]. When co-cultured with breast cancer cells in the presence of 5-FC, CD MSC were able to induce cell death, while Native MSC did not affect the cell viability for 6 days (Fig. 2d). Remarkably, CD MSC plated at a 1:2 ratio with cancer cells turned out to be as potent as 5-FU at inducing cancer cell killing for equal concentrations of 5-FC and 5-FU. Pictures of the co-culture, at day 6, showed a confluent cell layer with healthy cancer cells expressing RFP in presence of Native MSC, whereas in the presence of CD MSC and 400 μg/mL 5-FC, there were only a few apoptotic cancer cells left (Supplementary Fig. 6c).

3.2. Enhanced homing of engineered MSC to breast cancer bone metastases *in vivo*

Our engineered MSC's homing using PSGL-1/SLEX (not otherwise expressed on Native MSC), which targets bone niche selectins, recapitulates the bone homing cascade of haematopoietic stem cells (HSC) [43,48] and circulating tumour cells [49]. We next assessed the homing ability of our engineered MSC to breast cancer bone metastases *in vivo*. For this experiment, to mimic the clinical setting of patients with established bone metastases, we first used an immunocompromised animal model, in which human breast tumours were grown locally within the marrow cavity of the left tibia. Intratibial injection of breast cancer cells, to establish bone metastases, is a widely-used model to evaluate therapeutic intervention [50]. This route of injection was initially chosen in our study because it allowed us to develop robust and relatively homogenous tumours in the bone so that we could efficiently investigate MSC homing and treatment efficacy. We first checked the selectin expression within the tumour niche and found high expression of P-selectin in the bone marrow of the tumour leg (Fig. 3), but to a lesser extent in the healthy leg (Supplementary Fig. 7). We observed an inverse correlation between P-selectin expression and distance from the tumour site when we analysed P-selectin expression in the tumour legs of seven different animals (Fig. 3a,d). We observed large cells and smaller aggregates that highly express P-selectin, which we further identified to be megakaryocytes recruited to the tumour inflammatory site and their shed platelets, respectively, according to CD41 expression [25] (Fig. 3b). P-selectin expression is also observed on blood vessel endothelium, as shown by endomucin expression, a vascular marker (Fig. 3c).

A mock injection with PBS was performed in the healthy leg during the model induction. Once breast cancer bone metastases were established in all animals (typically 2 weeks post-implantation, around total bioluminescent signal 10^7–10^8 p/s), and the inflammation caused by injection had been mostly resolved [51], 7×10^5 Native or PSGL-1/SLEX/CD/OPG 24 h post-engineered MSC, pre-labelled with lipophilic dye (DiD), were injected *i.v. via* the tail vein. Mice were euthanised at 6, 24, 48 and 72 hours post cell transplantation. Legs and several relevant organs (lungs, liver, spleen, kidneys and heart) were isolated to measure the fluorescence emitted by DiD-MSC, using IVIS fluorescence imaging, to determine cell bio-distribution (Fig. 4, Supplementary Fig. 8). PSGL-1/SLEX/CD/OPG MSC showed significantly increased migration to the tumour leg compared to Native MSC ($p < .05$, Kruskal-Wallis with Dunn's multiple comparison test) at 72 hours post-implantation (Fig. 4a), although we did not observe any significant homing preferentially to the tumour leg *versus* healthy legs from the same animals. Over the combined time-points, PSGL-1/SLEX/CD/OPG MSC were significantly more localised in the mouse legs than Native MSC (Supplementary Fig. 9a). We confirmed the cell integrity of the PSGL-1/SLEX/CD/OPG MSC that had homed to the bone marrow using fluorescent microscopy (Supplementary Fig. 9b-c). These findings justify the use of PSGL-1/SLEX engineering, to maximise the number of MSC that reach the tumour site. Moreover, when analysing the bone marrow for P-selectin expression and MSC content, we found that PSGL-1/SLEX/CD/OPG MSC tend to accumulate in areas with high vascular P-selectin expression (Fig. 4b), which are usually found around the tumour site (Fig. 3a-d). In fact, the number of PSGL-1/SLEX/CD/OPG MSC (but not Native MSC) that migrated to the bone marrow positively correlates with P-selectin expression (Pearson coefficient $r = 0.7643$, $p < .0001$) (Fig. 4c), suggesting the active PSGL-1/SLEX and P-selectin axis drives the homing of PSGL-1/SLEX/CD/OPG MSC to the bone marrow. Moreover, we also characterised the bio-distribution of Native and PSGL-1/SLEX/CD/OPG MSC in other organs, and noticed that they initially accumulated in the lungs and liver within 24 hours post-transplantation, and were then rapidly cleared (Supplementary Fig. 8), which is consistent with previous studies [52,53].

Next, since the immune system could contribute to the clearance of transplanted MSC, we investigated the homing of PSGL-1/SLEX/CD/OPG MSC in a second, syngeneic, mouse model. This syngeneic model leads to spontaneous bone metastases, thus avoiding any potential inflammation created by needle insertion through the growth plate, such as during the intratibial model. We first identified a bone specific LucF/RFP 4T1 mouse breast cancer cell clone (CLL1) (see Methods). CLL1 (10,000 cells) were injected systemically, through the caudal artery, and within a week, small, but detectable bone metastases formed, preferential to

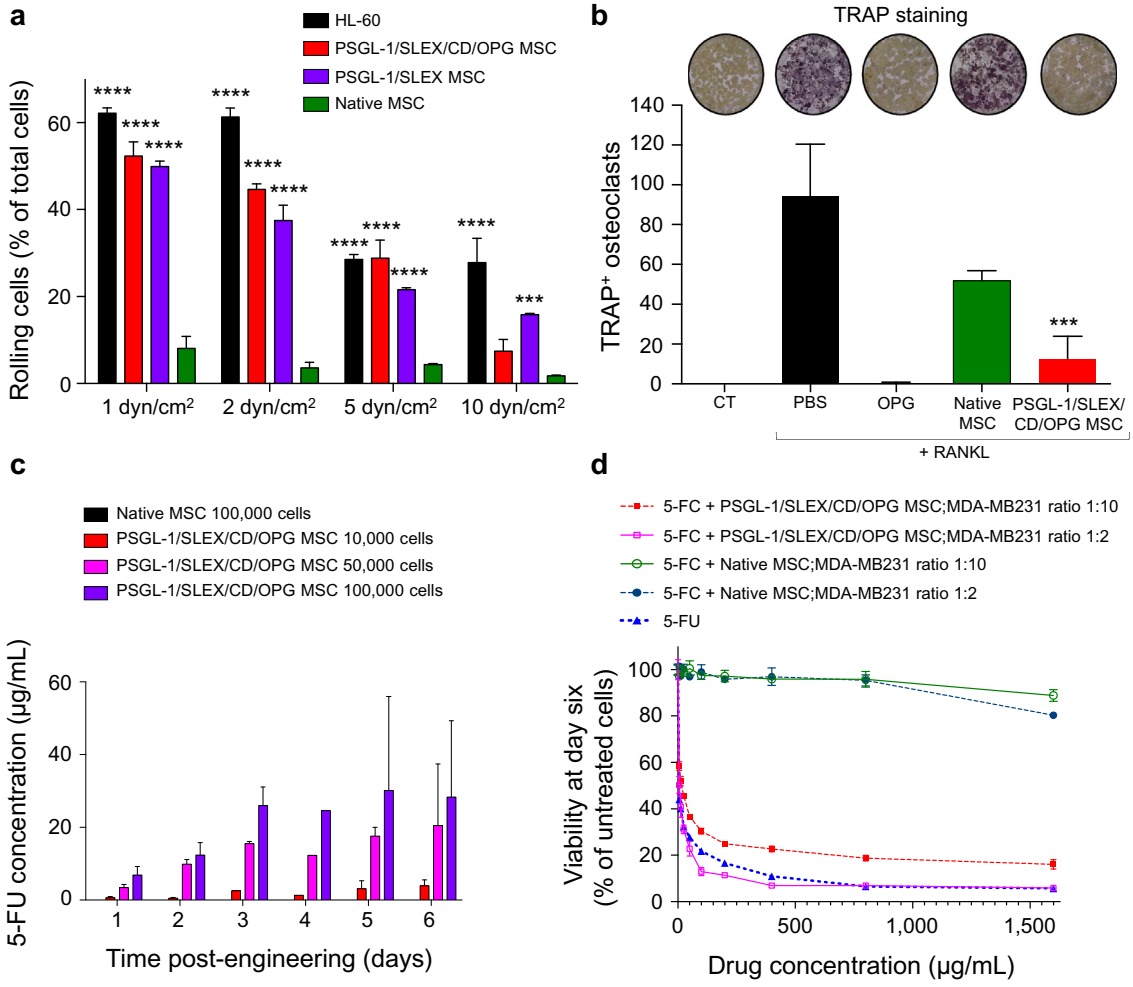

Fig. 2. MSC engineering using mRNA and *in vitro* functional validation. (a) PSGL-1/SLEX/CD/OPG MSC display functional rolling on an endothelial layer under physiological shear flow. Native MSC, PSGL-1/SLEX MSC and PSGL-1/SLEX/CD/OPG MSC were flowed on a layer of endothelial cells at different physiological flow-rates 24 h post-MSC engineering. HL-60 leukocytic cells were used as a positive control for rolling. Plot: mean + SD, statistical analysis: Two-way ANOVA test with Dunnett's multiple comparison test to compare each column to Native MSC, *** $p \leq .001$, **** $p \leq .0001$. (b) PSGL-1/SLEX/CD/OPG MSC inhibit osteoclastic differentiation *in vitro*. Murine osteoclast precursors (RAW264.7 cells) were plated for 6 days in media with no additional treatment (CT), 100 ng/mL recombinant murine RANKL to induce osteoclastogenesis, and day 2 supernatant of MSC (Native and PSGL-1/SLEX/CD/OPG). 100 ng/mL of recombinant human OPG was used as a positive control for osteoclastogenesis inhibition. Pictures show the TRAP stained culture at day 6 for each condition. Plot: mean + SD, statistical analysis: Kruskal-Wallis with Dunn's multiple comparison test, *** $p \leq .001$ compared to PBS + RANKL condition. (c) PSGL-1/SLEX/CD/OPG MSC convert 5-FC into 5-FU *in vitro* in a cell concentration-dependent manner. 24 h post-engineering, MSC were plated at different concentrations in presence of 400 µg/mL 5-FC. LC-MS/MS was done on conditioned media collected at different days to measure the 5-FU converted from 5-FC. Plot shows mean + SD. (d) PSGL-1/SLEX/CD/OPG MSC kill MDA-MB231 cancer cells *in vitro*. Native MSC and PSGL-1/SLEX/CD/OPG MSC were plated at different ratios (1:2 and 1:10) on top of cancer cells in the presence of increasing doses of 5-FC, and the viability of the co-culture was determined at day 6. 5-FU was used as a positive control. Graph shows mean ± SD.

the hind limbs and spine, as previously described [37]. The incidence of this model is excellent (>90% of animals developed bone metastases), but the model is very aggressive and mice usually have to be euthanised within 3 weeks. For this study, we aimed to further investigate engineered MSC homing to healthy legs *versus* tumour legs. As we were working with mouse tissue, we used Alu qPCR following an established approach [42] to detect human MSC in the leg. Despite the limited sensitivity of our protocol (see Methods), we were still able to detect PSGL-1/SLEX/CD/OPG MSC in 30% of the tumour legs, while none were detectable in the healthy legs. Up to 1156 MSC were detected per tumour leg 72 hours post transplantation, despite potential immune clearance in these immunocompetent animals (Supplementary Fig. 9 d, e).

3.3. Engineered MSC with both CD and OPG exhibit therapeutic effects in treating bone metastases in MDA-MB231 xenograft intratibial model

We then sought to determine the therapeutic efficacy of MSC further engineered with CD, OPG, or both factors to examine if 1) our therapy is efficient *in vivo*, in a breast cancer bone metastasis model, and 2) if such combinatorial delivery is more beneficial than either therapeutic alone. After verifying the presence of the tumour within the tibia of mice (typically 2 weeks post cancer induction), we injected 1×10^5 MSC engineered with CD (PSGL-1/SLEX/CD MSC), OPG (PSGL-1/SLEX/OPG MSC), CD/OPG (PSGL-1/SLEX/CD/OPG MSC) or Mock-transfected MSC into the tumour-bearing tibia (curative model) (Fig. 5a). PBS was injected in the control group (CT), as well as in the healthy legs (mock control for needle-induced inflammation and bone damages). We chose to use a local injection in this set of experiments, to allow for robust comparison between each treatment condition. The primary goal of this intratibial treatment injection was to test the efficacy of OPG and CD treatments, not to determine MSC homing (although the therapeutically engineered cells were also equipped with PSLG-1/SLEX, which replicates our final product, to be used in the systemic infusion in the following experiments). Mice were treated with 500 mg/kg of 5-FC pro-drug at 48 hours post-implantation, by which time MSC would have been cleared from filter organs if administered systemically as in our intended future clinical use.

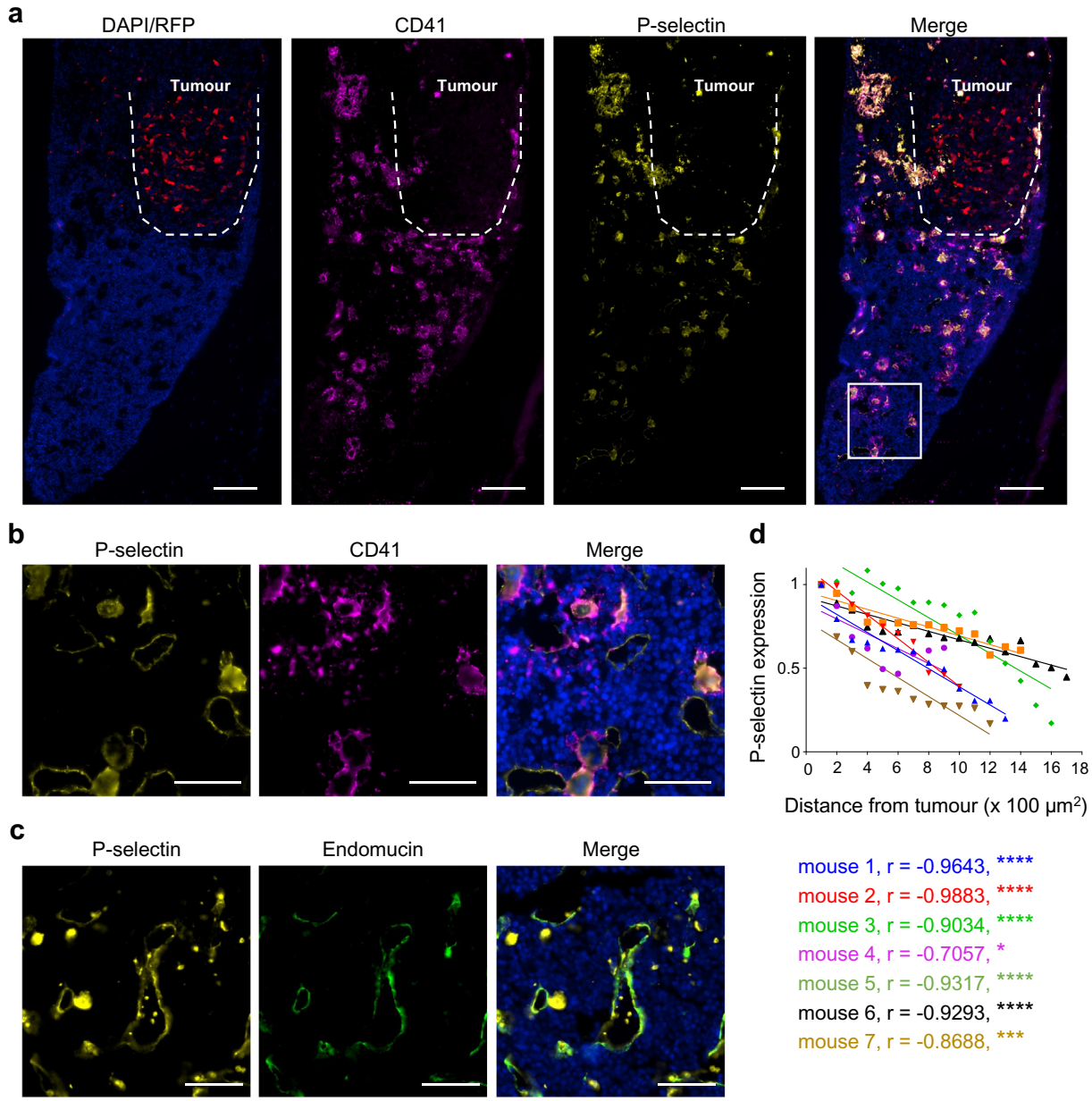

Fig. 3. P-selectin is highly expressed in the bone metastatic niche. (a) Both high P-selectin expression and elevated megakaryocytes/platelets number are seen in the bone marrow surrounding the tumour. Red: RFP constitutively expressed by tumour cells. Yellow: P-selectin, magenta: CD41 and blue: nuclei (DAPI staining). Dashed line outlines the tumour. The area designated by a white rectangle is showed at higher magnification in panel B. Scale bar: 100 µm. (b) Platelets and megakaryocytes express high level of P-selectin. Yellow: P-selectin, magenta: CD41 and blue: nuclei (DAPI staining). Scale bar: 50 µm. (c) P-selectin is expressed at the bone marrow endothelium in the breast cancer bone metastatic environment. Yellow: P-selectin, green: endomucin (vascular endothelium) and blue: nuclei (DAPI staining). Scale bar: 50 µm. (d) P-selectin expression is higher around the tumour area than in the rest of the bone marrow. P-selectin expression was quantified from bone marrow sections of 7 mice per area of 100 µm² from the tumour. r = Pearson correlation coefficient. * $p \leq .05$, *** $p \leq .001$, **** $p \leq .0001$.

A pilot experiment was first performed using $n = 4$ mice per group. Through this initial experiment, we established techniques to confirm tumour implantation within the tibia by overlaying bioluminescence and X-Ray (Supplementary Fig. 10a) and to characterise the presence of tumour cells within the bone marrow of the tibia by using both immunofluorescence (RFP expressed by cancer cells) and H&E staining (Supplementary Fig. 10b). From this experiment, we obtained a preliminary assessment on tumour killing and bone preservation among different treatment groups and determined the minimum number of mice per group required for statistical analysis using a power analysis (see Methods). We then repeated the experiment following the exact same treatment scheme (Fig. 5a) with $n = 10$ mice per group. Tumour growth within the tibia was monitored using bioluminescence imaging. Animals were randomised in each group and showed comparable tumour signal across groups before treatment (Supplementary Fig. 11). A tumour decrease was observed for animals treated with MSC engineered with both CD MSC groups, particularly CD/OPG MSC ($p < .05$ from Kruskal-Wallis with Dunn's multiple comparison *post hoc*, compared to Mock MSC), immediately following the treatment (Fig. 5b, c), but most of the tumours eventually grew back to a level comparable to control groups (PBS and Mock MSC). At the end-point, mice treated with CD/OPG MSC also exhibited smaller tumours compared to control groups (although the difference was not significant, due to high variability between good and bad responders). However, OPG MSC slowed the tumour growth, leading to significantly smaller tumours than the Mock MSC group ($p < .05$, Kruskal-Wallis with Dunn's multiple comparison *post hoc*) in the longer-term (Fig. 5b, d, Supplementary Fig. 11). In addition, we analysed the tumour growth data

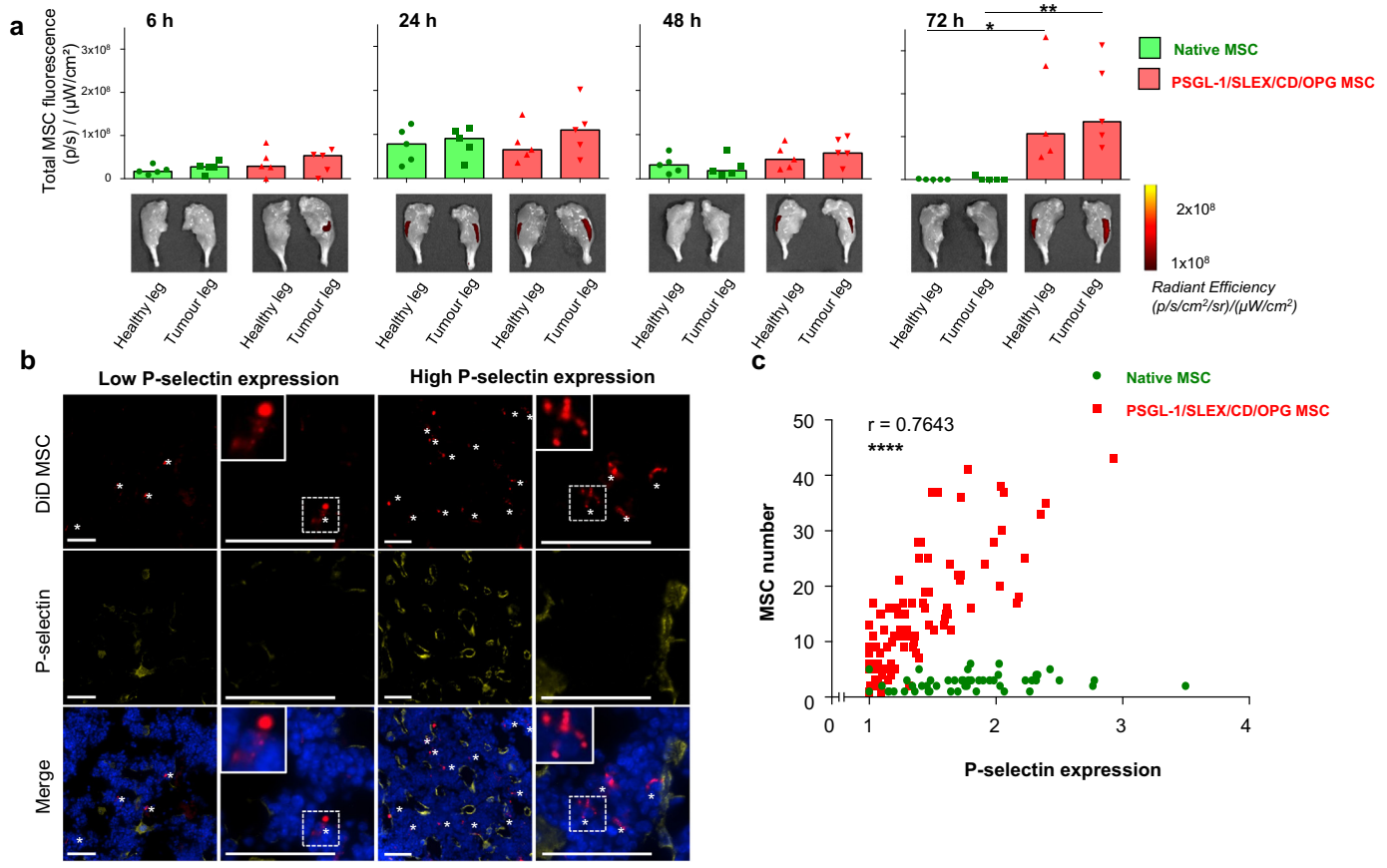

Fig. 4. Enhanced homing of engineered MSC to breast cancer bone metastases *in vivo* in the MDA-MB231 intratibial model. (a) PSGL-1/SLEX/CD/OPG MSC display an increased homing to the tumour legs 72 h post-transplantation. Native MSC or PSGL-1/SLEX/CD/OPG MSC labelled with DiD lipophilic dye were injected *i.v.*, then mice were euthanised at different time-points (6, 24, 48, and 72 h). Homing to the legs was evaluated based on the fluorescence intensity of the DiD dye. Control animals that were not injected with MSC were used to subtract fluorescent background from true signal. Plot: median values, each point is an individual animal, $n = 5$ animals per group, statistical analysis: Kruskal-Wallis with Dunn's multiple comparison test * $p \leq .05$ between Native MSC (healthy leg) and PSGL-1/SLEX/CD/OPG MSC (healthy leg), ** $p \leq .01$ between Native MSC (tumour leg) and PSGL-1/SLEX/CD/OPG MSC (tumour leg). (b) PSGL-1/SLEX/CD/OPG MSC accumulate in high P-selectin expression areas in the bone marrow section (48 h post-transplantation time-point). Red: DiD stained MSC, yellow: P-selectin, blue: nuclei (DAPI staining). White stars designate MSC. Scale bars: 50 μm. (c) PSGL-1/SLEX/CD/OPG MSC number within the bone marrow is positively correlated to P-selectin expression. 200 μm by 200 μm areas containing MSC were selected for quantification from the 72 h time-point post-MSC transplantation. Average P-selectin signal was measured by dividing total photon counts emitted in Cy5 per surface area and subtracting the background signal. 49 areas were evaluated for Native MSC, and 95 areas were assessed for PSGL-1/SLEX/CD/OPG MSC. Statistical analysis: Pearson correlation test, coefficient $r = 0.7643$, **** $p \leq .0001$ for PSGL-1/SLEX/CD/OPG MSC.

points from both pilot and larger-scale experiments using a linear mixed model (LMM), which takes inter-experiment variability into account (Supplementary Table 3). This LMM analysis showed CD/OPG MSC treatment is most effective among all engineered MSC groups in decreasing tumour growth both immediately after treatment ($p = .0039$), and at the end-point ($p = .0494$), compared to the PBS control as it was used in both studies.

We further investigated tumour-induced bone damage by analysing bone structure of all tibias at the end-point, using microcomputed tomography (micro-CT). One representative animal from each group, which exhibited the closest values to the median of that group for the bone analysis, was presented in Fig. 5e. The 3D reconstruction of the entire tibias clearly indicated extensive bone damage in the PBS and Mock MSC treated groups, while damage looked less severe in engineered MSC treated groups, in particular for animals treated with OPG MSC (Supplementary Video 2). As tumours grow inside the bone marrow cavity before invading the cortical bone, we also looked at the trabecular bone, which was mainly gone in most of the groups, except for the OPG MSC treated mice, which exhibited trabecular bone structure similar to the one found in healthy legs (Fig. 5e, Supplementary Video 3). We further quantified the trabecular bone left in each tumour-bearing tibia, and illustrated the bone loss, by normalising the obtained values to the trabecular bone volume of healthy legs (Fig. 5f). Indeed, 70% of the mice from OPG MSC group had <50% trabecular bone loss, thus exhibiting significant protection against tumour-induced bone loss compared to Mock MSC group ($p < .05$, Kruskal-Wallis with Dunn's multiple comparison *post hoc*). We also performed histology on the tumour-bearing tibias from those animals (five representative animals from each group as shown in Fig. 5g). Control groups (PBS and Mock MSC) showed extensive tumour invasion through the cortical bone, with total loss of bone architecture in some cases. In contrast, bone structure was preserved for good responder animals treated with engineered MSC, in particular in the OPG MSC group, where the tibias look healthier than for the other groups. Moreover, the LMM analysis of trabecular bone, from both pilot and larger-scale experiments, showed that both OPG MSC and CD/OPG MSC displayed significantly less trabecular bone damage than the PBS control group, with the OPG MSC being the most effective in protecting against tumour-induced bone damage (Supplementary Table 4). Furthermore, we evaluated the impact of OPG MSC treatment in inhibiting tumour-induced osteoclastogenesis *in vivo* using tartrate-resistant acid phosphatase (TRAP) staining for osteoclasts in the growth plate of the tibias of mice (both healthy and tumour legs) (Supplementary Fig. 12). Healthy legs of tumour mice treated with PBS were included as a control. Note that we could not include tumour legs, as the growth plates were gone, due to tumour invasion and high osteoclastic activity [3] (Fig. 5g). We found that the

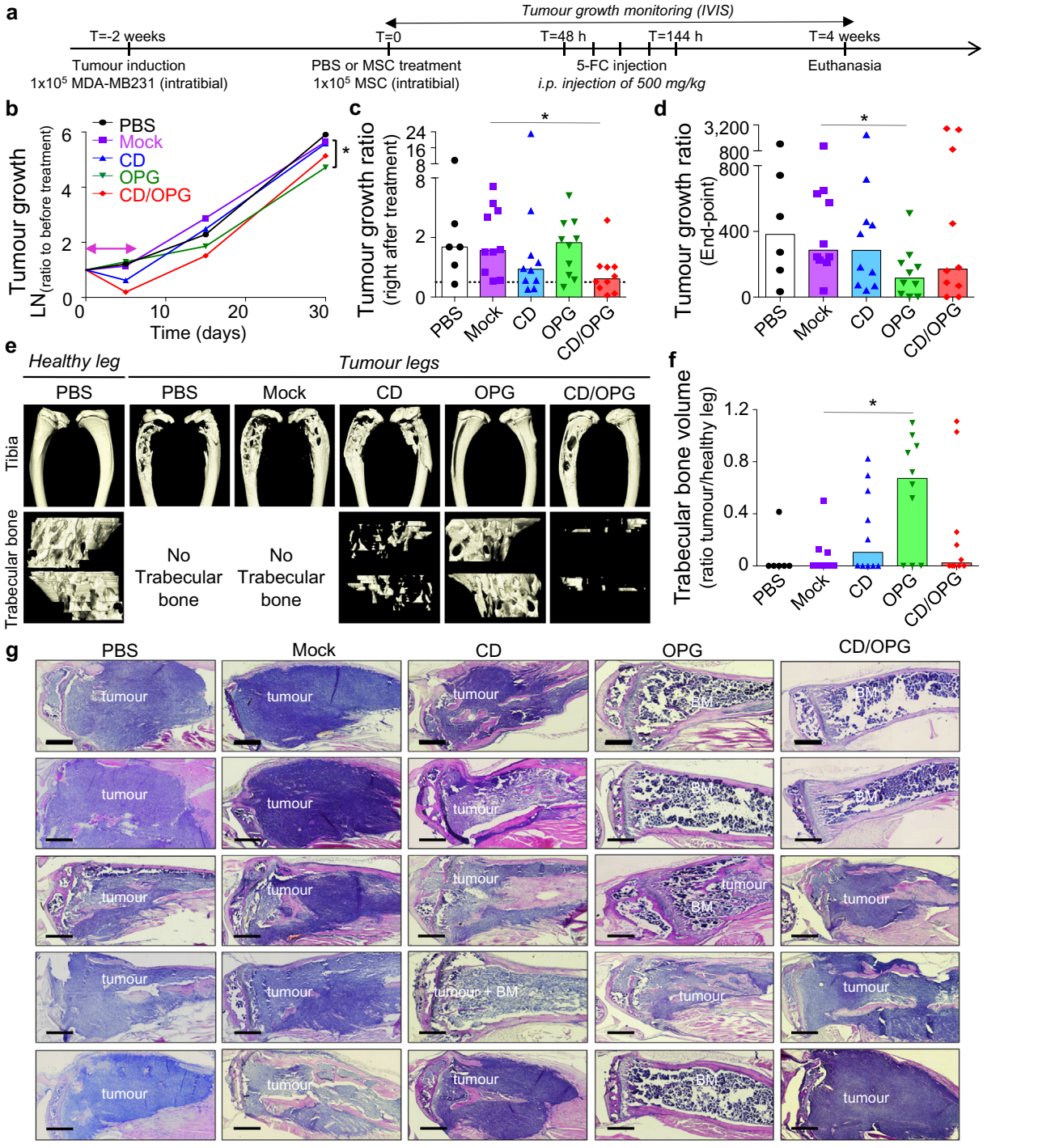

Fig. 5. Engineered MSC exhibit therapeutic effects in treating bone metastases *in vivo* in the MDA-MB231 intratibial model. (a) Timeline of the therapeutic treatment validation. MSC were engineered as follows: Mock group (Mock transfected), CD group (PSGL-1/SLEX/CD), OPG group (PSGL-1/SLEX/OPG) and CD/OPG group (PSGL-1/SLEX/CD/OPG) and injected directly into the tibia, $n = 10$ per group. PBS group only received PBS in the tibia instead of MSC, $n = 6$. (b) The logarithm values of the tumour growth ratio (Total photon flux measured/Total photon flux on the day before the treatment started) are plotted over time for each group. Median of each group is shown. Pink double-headed arrow shows treatment duration. Statistical analysis: Kruskal-Wallis with Dunn's multiple comparison *post hoc*, * $p \leq .05$ between Mock MSC and OPG MSC. (c) Bar graph shows the tumour growth ratio measured on the day after the treatment is done. Each point represents one animal, and the bars represent the median value of the group. Dashed line indicates a tumour growth ratio of 1 (animals below that line have tumour decrease). Statistical analysis: Kruskal-Wallis with Dunn's multiple comparison *post hoc*, * $p \leq .05$ between Mock MSC and CD/OPG MSC. (d) Bar graph shows the tumour growth ratio measured on the end-point day. Each point represents one animal, and the bars represent the median value of the group. Statistical analysis: Kruskal-Wallis with Dunn's multiple comparison *post hoc*, * $p \leq .05$ between Mock MSC and OPG MSC. (e) MicroCT imaging was done on mouse tibias after euthanasia. Representative 3D reconstructions matching the median of each group for bone analysis are shown. First row shows whole tibias without the fibula, while bottom row shows trabecular bone. (f) Bar graph shows the trabecular bone ratio measured by normalising the trabecular bone volume of each tumour leg to the trabecular bone volume of healthy legs. Each point represents one animal, and the bars represent the median value of the group. Statistical analysis: Kruskal-Wallis with Dunn's multiple comparison *post hoc*, * $p \leq .05$ between Mock MSC and OPG MSC. (g) H&E staining of mouse tibias at end-point demonstrate treatment with OPG MSC and CD/OPG MSC can clear tumour cells and preserve the bone structure, while tumour invades the cortical bone in control animals (PBS and Mock MSC groups). 5 representative mouse tibias are shown for each group. BM = healthy bone marrow. Scale bar: 500 μm.

number of TRAP$^+$ osteoclasts was significantly reduced in the tumour tibias from the mice treated with OPG MSC compared to the PBS control ($p < .05$, Kruskal-Wallis with Dunn's multiple comparison *post hoc*). Finally, in this experiment (Fig. 5), we observed OPG MSC exerted a stronger therapeutic effect than CD/OPG MSC. This could be because CD/OPG MSC has lower expression levels of therapeutic proteins due to engineering with multiple factors compared to OPG MSC. Nevertheless, the data above suggest that both CD (in short term) and OPG (in long term) exhibit therapeutic effects *in vivo*, but their co-expression should be further investigated to maximise their combinatorial effect in inhibiting both tumour growth and preserving bone integrity. We reason that even if OPG MSC were able to slow down tumour growth, they could not clear the tumour as CD MSC do, justifying the potential benefit of combination therapy. After all, the LMM analysis suggested potential benefit of the CD/OPG MSC combined therapy. Therefore, we decided to use the combination treatment PSGL-1/SLEX/CD/OPG MSC for the following intravenous (*i.v.*) administration studies. As our envisioned treatment in the clinic will be an off-the-shelf cell therapy administered *via* simple *i.v.* infusion, we next assessed efficacy, with a focus on survival, and systemic toxicity of our PSGL-1/SLEX/CD/OPG MSC following *i.v.* delivery. We compared their tumour-killing effect to a toxic dose of the chemotherapeutic drug 5-FU, a common treatment for breast cancer patients known for its side-effects [47]. As illustrated in Fig. 6a, we intravenously injected our engineered MSC through the tail vein, followed by daily treatment with 500 mg/kg 5-FC intraperitoneally (*i.p.*), starting 48 hours post-transplantation over 5 days. The control group consisted of tumour bearing animals only injected with PBS. In another group, 200 mg/kg 5-FU was injected *i.p.* on the same schedule as the 5-FC group. This relatively high dose of 5-FU was used as a positive control for tumour killing and tissue toxicity, as previous studies we performed with lower doses (up to 50 mg/kg for five days during three consecutive weeks) neither induced toxicity nor killed MDA-MB231 xenografts in Nude animals [54]. We also included a triple MSC injection group to examine if multiple injections perform better than single injection; in this case, the treatment schedule was repeated for three consecutive weeks. 3 to 4 mice per group were sacrificed at the end of the treatment to evaluate tissue toxicity, while the rest of the mice were kept for long-term survival analysis. The overall survival of control animals or animals treated with Native MSC was very similar, with all the animals euthanised by 50 days (Fig. 6b). The toxicity of 5-FU was so severe that all animals died or had to be euthanised by day 10. Notably, around day 7, the 5-FU treated mice stopped grooming, started having diarrhoea and showed dramatic weight loss, indicating signs of toxicity. By contrast, mice treated with MSC did not show any sign of distress and gained weight during the experiment similar to the control mice. Importantly, their survival was significantly improved by the treatment, in particular for the triple injection group where 30% of the mice were still alive after 111 days, *versus* 12.5% for the single injection group (Fig. 6b).

In addition, at the time of euthanasia, we observed a noticeable reduction (about 2/3) of the size of spleens in the 5-FU group compared to the control group, whereas MSC treatment did not seem to affect the spleen size and morphology (Supplementary Fig. 13a). H&E analysis of spleen sections confirmed tissue damage induced by 5-FU, with a decrease of the size of germinal centres, replaced by fibrotic tissue (Fig. 6c-d, Supplementary Fig. 13b). In regard to toxicity to other organs, including lungs, liver, kidney, bone marrow, and small/large intestines, we observed reduction of the size of villi in the small intestine and a decrease of the number of goblet cells per villus. Severe haemolysis happened in the bone marrow for the 5-FU group with a decrease of the number of leukocytes, while no significant difference in tissue structure was observed among groups for the other organs (Fig. 6c–d, Supplementary Fig. 14). In addition, we isolated the bone marrow to analyse the general cell viability and the different populations using flow cytometry. Consistent with our previous conclusions, PSGL-1/SLEX/CD/OPG MSC did not induce significant cell death within the healthy bone marrow, unlike the 5-FU treatment [55], which considerably increased the percentage of necrotic cells (1.68 fold increase), and decreased the percentage of viable cells (2.71 fold decrease) compared to the CT group (Fig. 6e). Although the percentage of Annexin V$^+$ cells was not significantly different between each group, 5-FU induced stronger apoptosis with a median of fluorescence intensity (MFI) 4.8 times higher than that of the other groups for Annexin V FITC. The MFI for the 7-ADD$^+$ cells in the 5-FU group was also 16.7 times higher than the other groups, confirming an overall lower cell viability in the bone marrow of 5-FU treated animals (Supplementary Fig. 13c). Regarding the populations affected, we only observed a slight increase of B cells B220^{high} in the single injection group (5.24% *versus* 3%) (Fig. 6f). However, these changes are minimal compared to those induced by high-doses of 5-FU, which, unsurprisingly, induced a 3.84-fold decrease of the myeloid component, a 4.7-fold decrease of B220^{low} B cells and 14.8-fold increase of B220^{high} B cells within the bone marrow, compared to the control group [55]. Taken together, these results showed that our engineered MSC based therapy was able to extend the animals' survival without inducing significant systemic toxicity compared to high-dose 5-FU treatment. Finally, we performed preliminary assessment of the bone integrity, which demonstrated PSGL-1/SLEX/CD/OPG MSC exhibited a promising protective effect on bone damage, compared to the Control (PBS) and Native MSC groups (Supplementary Fig. 15, Supplementary Table 5). With this encouraging preliminary study, we decided to extensively investigate our engineered MSC's therapeutic effects in killing tumour cells and protecting against bone loss, as well as its potential toxicity using a more clinically relevant animal model (immunocompetent, and of spontaneous bone metastasis, see below).

3.4. Engineered MSC with both CD and OPG exhibit superior therapeutic effects in a syngeneic model of spontaneous bone metastases

We next tested our engineered MSC therapy in our second syngeneic mouse model, which takes into consideration the immune system component and leads to spontaneous bone metastases (Supplementary Fig. 16a). We included PBS and Mock-transfected MSC, the combined therapy PSGL-1/SLEX/CD/OPG MSC (CD/OPG MSC), as well as the monotherapies PSGL-1/SLEX/CD MSC (CD MSC) and PSGL-1/SLEX/OPG (OPG MSC). We focused on two main outcomes for this study: efficacy and toxicity. A minimum number of 10 mice per group was determined by the power analysis; we included 10 animals for PBS, Mock-transfected MSC and 5-FU groups, while we used 13 animals in the CD MSC, OPG MSC and CD/OPG MSC groups. As soon as all animals had detectable bone metastases, we systemically injected engineered MSC groups, followed by 500 mg/kg 5-FC for 5 consecutive days, starting two days post MSC transplantation (Fig. 7a). PBS injections were done as a control. For a treatment reference, we injected 5-FU *i.p.* with a clinically relevant dose of 12.5 mg/kg [38] (see Methods for dose optimisation), following the same schedule as for 5-FC injections. We first evaluated the efficacy by measuring the tumour growth ratio over time (total photon flux divided by the total photon flux measured before treatment for each animal). PBS was used as a control since MSC transplantation could induce an immune response in this model, thus not being an appropriate control. Although initially very small, tumours developed extremely rapidly (Supplementary Fig. 16a). Among the groups tested, only the CD/OPG MSC treatment was able to induce a significant tumour decrease, as determined by a non-parametric ANOVA at the end-point ($p < .05$ between PBS and CD/OPG groups) (Fig. 7b). We further investigated the differences between the combined therapies and the monotherapies and plotted the tumour growth ratio at the end-point, for each animal, for CD and CD/OPG groups as well as for OPG and CD/OPG groups (Supplementary Fig. 16b and c). We noticed several populations based on response to treatment, with a clear good responder group for the mice treated by CD/OPG MSC, which was absent in groups treated by CD MSC or OPG MSC. The combined therapy was more efficient in preventing tumour growth than CD MSC

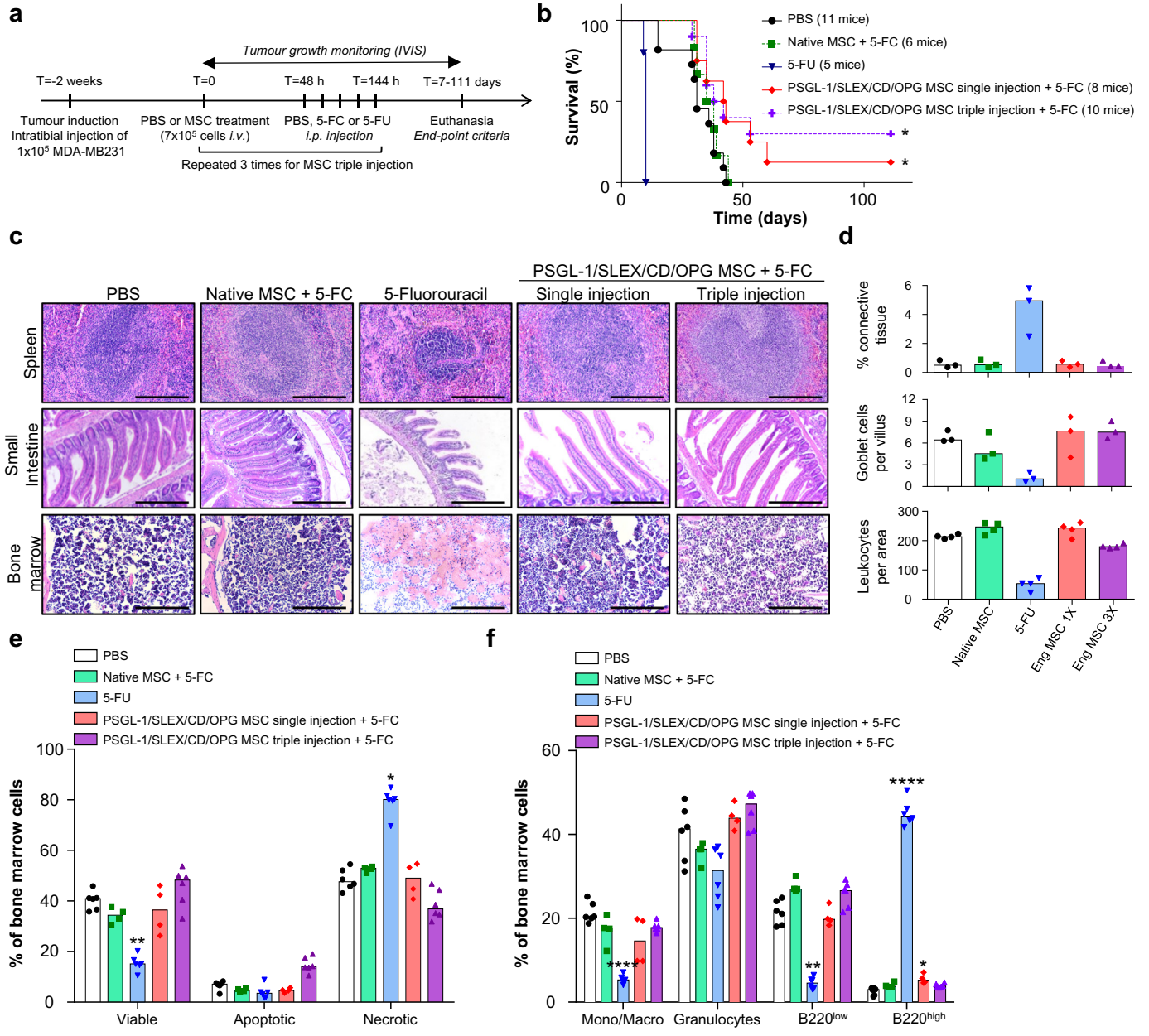

Fig. 6. Systemic infusion of PSGL-1/SLEX/CD/OPG MSC improves animal survival without inducing systemic toxicity in the MDA-MB231 intratibial model. (a) Timeline of the therapeutic treatments. PBS or 7×10^5 MSC (Native or PSGL-1/SLEX/CD/OPG) were injected *i.v.* and 48 h later 500 mg/kg 5-FC or 200 mg/kg 5-FU was injected *i.p.* once a day for 5 days. Mice were euthanised as defined by end-point criteria (total photon flux $>10^{10}$ p/s, signs of pain or distress, *etc.*). (b) PSGL-1/SLEX/CD/OPG MSC treatment improves overall animal survival. The graph shows the percentage of survival of the animals in the different groups: CT (PBS control, 11 mice), Native MSC + 5-FC treatment (6 mice), 5-FU (5 mice), PSGL-1/SLEX/CD/OPG MSC single injection +5-FC treatment (8 mice) and PSGL-1/SLEX/CD/OPG MSC triple injection +5-FC treatment (10 mice). Statistical analysis: Log-rank (Mantel-Cox) test, * $p \leq .05$. (c) PSGL-1/SLEX/CD/OPG MSC treatment group exhibits minimal systemic toxicity compared to 5-FU treatment. Tissue analysis was performed following H&E staining to evaluate toxicity-induced damage. Panel shows organs where the greatest damage was observed: spleen, small intestine, and bone marrow. Scale bars: 500 μm for spleen and bone marrow, 250 μm for the small intestine. (d) Engineered MSC did not induce significant tissue damage. Quantifications were done on the H&E staining: percentage of connective tissue to assess spleen fibrosis, number of goblet cells per villus to evaluate intestine damage, and number of leukocytes per bone marrow area to measure toxicity. Bar graph shows the median for each group, and each point represents one animal, $n = 4$ mice per group. Eng MSC = PSGL-1/SLEX/CD/OPG MSC. (e) Engineered MSC did not lead to significant cell death in the bone marrow. Flow cytometry was performed on bone marrow to analyse the percentages of viable, apoptotic and necrotic cells. 2 to 3 animals were used for each group, and both legs were analysed. As no major differences were observed between the healthy and the tumour leg, data from both legs were pooled. Bar graph shows the median for each group, and each point represents one analysed leg. Statistical analysis: Kruskal-Wallis followed by a Dunn's multiple comparison test among each group (viable, apoptotic and necrotic) to compare all conditions to the control; * $p \leq .05$, ** $p \leq .01$. (f) Engineered MSC did not significantly alter cell composition of the bone marrow. Flow cytometry was performed on equal numbers of bone marrow cells to analyse the different populations: monocytes/macrophages (Mono/Macro), granulocytes and B lymphocytes ($B220^{low}$ and $B220^{high}$). 2 to 3 animals were used for each group, and both legs were analysed. As no major differences were observed between the healthy and the tumour leg, data from both legs were pooled. Bar graph shows the median for each group, and each point represents one analysed leg. Statistical analysis: Kruskal-Wallis followed by a Dunn's multiple comparison test among each population to compare all conditions to the control; * $p \leq .05$, **** $p \leq .0001$.

monotherapy ($p < .05$, Kruskal-Wallis with Dunn's multiple comparison *post hoc*), and also tends to be more efficient than OPG MSC therapy ($p = .0638$, Kruskal-Wallis with Dunn's multiple comparison *post hoc*). Moreover, mice treated by CD/OPG MSC seemed healthier than other groups overall, with less moribund mice, better grooming and ability to move around, at the end-point (Supplementary Video 4). Due to the aggressiveness of this model, mouse condition deteriorated extremely rapidly (paraplegia and diarrhoea due to spine metastasis,

weight loss, and tumours breaking through the cortical bone). We decided to score the paralysis to quantify this effect, and confirmed that CD/OPG MSC treated mice were less paralysed than mice in PBS control group ($p < .05$, Kruskal-Wallis with Dunn's multiple comparison *post hoc*), with the majority of mice being free of movement, while the majority of animals in other groups were dragging their hind limbs (Fig. 7c). We then examined treatment effects on tumour-induced bone damage for those animals, and randomly picked 6 animals per groups, which possessed clear bone metastatic signal coming from the leg before the treatment. As a majority of bone metastases found in the hind limbs were located in the hip and femur area, we decided to focus on the femurs, instead of the tibias, for this model (Fig. 7D, Supplementary Video 5). For each sample, we asked twenty people (75% of them not being familiar with this study or not doing research) to blindly score the shaft damage and the epiphysis damage. The scoring matched the 3D reconstructions, with significantly less bone damage in the group treated with CD/OPG MSC ($p < .05$ analysed by Kruskal-Wallis with Dunn's multiple comparison *post hoc* test, between PBS and CD/OPG groups, Fig. 7e). In addition, we quantified the total bone volume and the remaining trabecular bone in the epiphysis. CD/OPG MSC and OPG

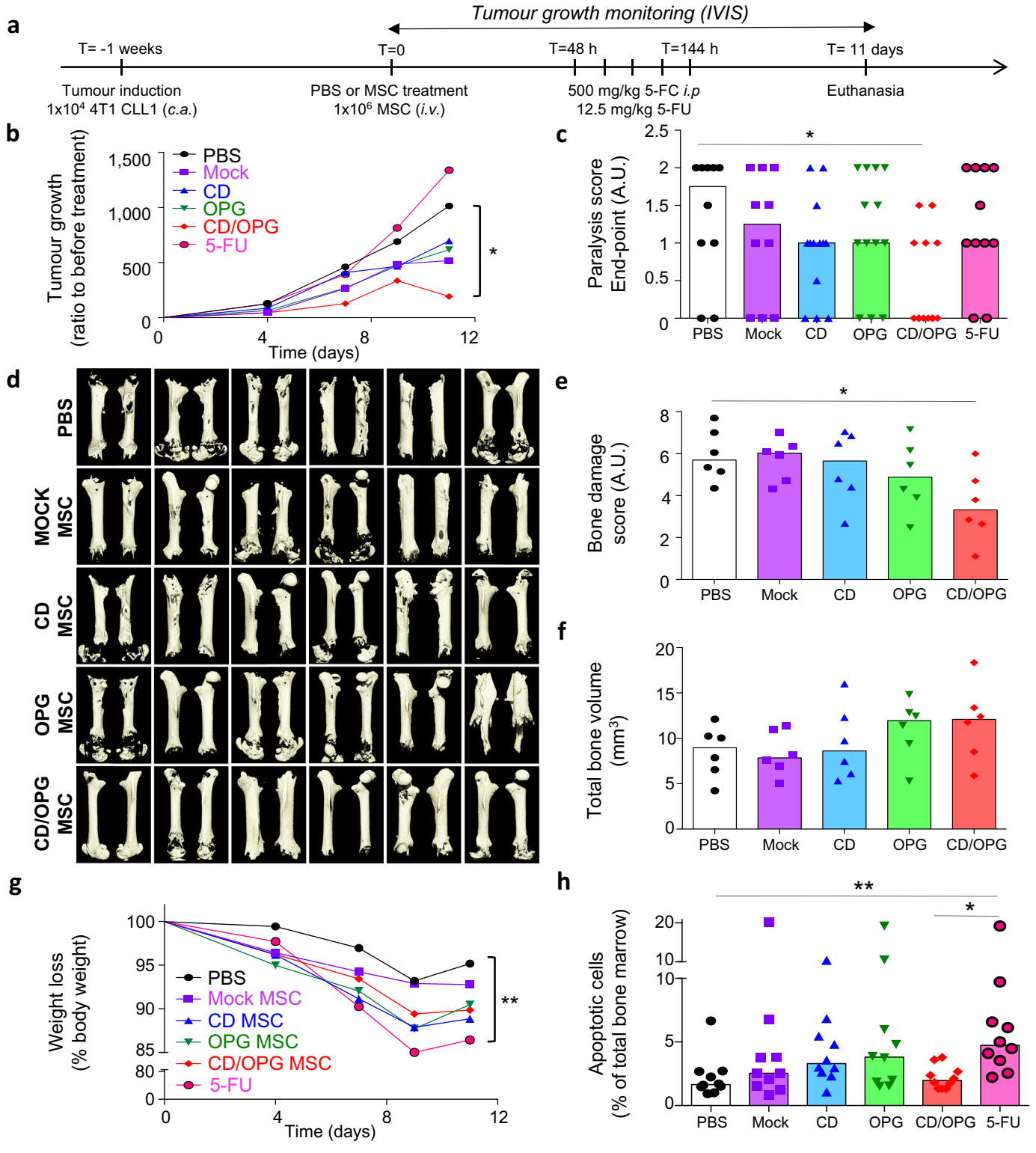

MSC tend to have more total bone volume than the PBS control (although the results were not significant) (Fig. 7f). Similarly, animals treated with CD/OPG MSC tended to have more remaining trabecular bone than the PBS control group ($p = .0748$ analysed by Kruskal-Wallis with Dunn's multiple comparison *post hoc* test, Supplementary Fig. 16d).

Our second goal was to evaluate potential toxicity of our engineered MSC. This time, we compared the toxicity of each treatment to our 5-FU reference. First, we measured the body weight of the animals during the whole experiment, and although all animals did lose weight because of the aggressive bone metastases, our engineered MSC therapies did not induce significant weight loss compared to the PBS group, while 5-FU did (Fig. 7g). Then, we performed H&E staining on peripheral organs, including spleen, intestines, and bone marrow, which did not exhibit any major toxicity among all treatment groups (Supplementary Fig. 16e). We also analysed the bone marrow of the mouse femur for 10 animals per group at the end-point, both for cell viability (Fig. 7h, Supplementary Fig. 16f), and myeloid cell population (Supplementary Fig. 16g). MSC groups had minimal effect on these measures, while 5-FU reference treatment exhibited significant toxicity. Taken together, these findings suggest that 1) our combined CD/OPG MSC therapy exhibited therapeutic efficacy in a syngeneic mouse model of bone metastasis, while monotherapies and 5-FU did not, and 2) our targeted approach is significantly less toxic than its non-targeted chemotherapy counterpart *in vivo*.

4. Discussion

Bone metastases are common, incurable, and associated with debilitating complications. Existing monotherapies and drug delivery systems are ineffective and often present severe side effects [2,8]. Efficient treatment of metastatic bone diseases requires simultaneous addressing of tumour growth and bone resorption. Although previous studies showed synergistic effects for breast cancer bone metastases treatment when combining bisphosphonates and chemotherapeutic agents [56,57], drug delivery and associated systemic toxicity remain a challenge. Here, we introduce a new paradigm of bone metastasis treatment by embracing a combination therapy that targets both the cancer cells and their niche through a stem-cell-based vehicle that homes to the bone tumour sites. We reasoned that such a combinatorial treatment targeting multiple cancer mechanisms would be of paramount importance to efficiently treat bone metastases along with preventing drug resistance, relapse, and development of new metastases compared to monotherapies, with limited side-effects. Indeed, by co-delivering both an anti-tumour agent (CD/5-FC pro-drug) [20] and an anti-osteolytic agent (OPG) [58], our engineered stem cell system displayed great potential in both killing tumour cells and preserving bone integrity. Given the current challenges in co-delivery of biologics in a controlled fashion, our mRNA-based cell engineering presents a simple and powerful way to target multiple mechanisms (tumour-selectin expression, tumour growth and bone resorption) simultaneously in a rapid and transient way following treatment, therefore avoiding potential long-term safety issues observed in traditional viral engineering approaches [59,60]. Previous studies targeting bone tumours through a cell-based therapy used genetically modified cells, which usually only delivered a single therapeutic molecule [29–31]. We showed that not only does mRNA engineering allow concurrent expression of multiple factors, but that it also leads to therapeutic efficacy similar to that of genetic engineering [19]. Moreover, safety concerns are limited regarding MSC persistence following transplantation as MSC are killed along with the surrounding cancer cells within days after converting 5-FC to 5-FU [19].

MSC represent ideal trophic vehicles for drug delivery to bone metastases as systemically delivered MSC have been shown to preferentially localise to, and subsequently integrate with the bone marrow [61], showing promising potential for bone tumour treatment [62]. Our system also takes advantage of the engineered homing of MSC to specifically and efficiently deliver 'cargo' to the target tumour site. This 'active' targeting circumvents many hurdles associated with conventional delivery systems (*i.e.*, by direct administration or nanoparticles), which cannot efficiently reach and penetrate metastatic sites [14]. By recapitulating the bone-homing cascade of HSC and metastatic cancer cells, we are able to maximise MSC delivery to bones, through interactions between PSGL-1/SLEX and selectins on activated bone vasculature [9], and on megakaryocytes and platelets [63], in the tumour area. Indeed, P- and *E*- selectins are overexpressed in many patients' tumours [64]. It is also interesting to note that PSGL-1/SLEX-engineered MSC could interact with circulating platelets, as observed in the leukocyte and tumour cell trafficking cascades [63,65,66], en route to the bone metastatic niche, which could further facilitate MSC delivery, and will be investigated in the future. This targeted approach would significantly minimise undesirable toxicity, as observed in treatment with chemotherapeutics, including 5-FU, in the clinic. Our results clearly showed that engineered MSC home more to the bone metastatic sites than Native MSC. Interestingly, we did not observe a significant difference in the homing of engineered MSC to tumour-bearing legs and to healthy legs overall, (whole leg imaging) in our first MDA-MB231 intratibial model. This could be due to the basal expression of selectins and/or activated selectin expression following needle-induced inflammation in the tibia, or tumour-induced systemic inflammation in the bone marrow vasculature of healthy legs [25,26]. In fact, we also noticed P-selectin expression within the bone marrow of the healthy leg of tumour-bearing mice, corroborating this hypothesis. We observed that MSC were sparse in the healthy leg, but in the tumour leg they were

Fig. 7. CD/OPG MSC exhibit therapeutic effects and minimal toxicity in a syngeneic mouse model of spontaneous bone metastasis. (a) Timeline of the therapeutic treatment. Spontaneous bone metastases were induced by caudal artery injection of a 4T1 bone metastatic clone (CLL1) to BALB/cJ mice. Once bone metastases were detected, engineered MSC or PBS were systemically administered to animals *via i.v.* injection, and 5-FC was injected *i.p.* for 5 consecutive days 48 h post transplantation. 12.5 mg/kg 5-FU was used as a reference group for treatment. MSC were engineered as follows: Mock group (Mock transfected), CD group (PSGL-1/SLEX/CD), OPG group (PSGL-1/SLEX/OPG) and CD/OPG group (PSGL-1/SLEX/CD/OPG). PBS, Mock and 5-FU groups: $n = 10$ animals per group. CD, OPG and CD/OPG groups: $n = 13$ per group. (b) CD/OPG MSC inhibits tumour growth compared to PBS control group. Bioluminescence imaging was performed over time and signal was quantified in the lower body to measure bone metastases development in legs and spine. The median of the tumour growth ratio (total photon flux over time normalised to total photon flux before treatment) was plotted for each group. Statistical analysis done at the end-point: Kruskal-Wallis with Dunn's multiple comparison *post hoc*, * $p \leq .05$ between PBS and CD/OPG MSC. (c) CD/OPG treatment improves mouse mobility. Paralysis of the animals was scored at the end-point (see Methods). Bar graph shows the median score for each group, and each point represents one animal. Statistical analysis: Kruskal-Wallis with Dunn's multiple comparison *post hoc*, * $p \leq .05$ between PBS and CD/OPG MSC. (d) Femurs bearing bone metastases are less damaged in CD/OPG MSC treated group. Micro-CT analysis was done on mouse femurs exhibiting clear leg metastases (usually around the hip area) before treatment from 6 mice per group. 3D reconstructions were made from the whole femurs. (e) Bone damage was blindly scored by a panel of 20 unbiased persons (shaft damage from 0 to 3 and epiphysis damage from 0 to 5 based on importance of damage). The average scoring was shown for each animal. Bar graph represents the median score for each group, and each point represents one animal. Statistical analysis: Kruskal-Wallis with Dunn's multiple comparison *post hoc*, * $p \leq .05$ between PBS and CD/OPG MSC. (f) CD/OPG MSC and OPG MSC treatments seem to protect against bone loss. The total bone volume was quantified for each femur. Bar graph shows the median bone volume for each group, and each point represents one animal. Statistical analysis: Kruskal-Wallis with Dunn's multiple comparison *post hoc*. (g) 5-FU treatment, but not MSC groups, induces significant body weight loss. Graph shows the median body weight loss for each group over time. Statistical analysis done at the end-point: Kruskal-Wallis with Dunn's multiple comparison *post hoc*, ** $p \leq .01$ between PBS and 5-FU. (h) Only 5-FU treatment induces additional apoptosis in the bone marrow. At the end-point, the bone marrow of the healthier leg was isolated and cell apoptosis was analysed using flow-cytometry (AnnexinV+/7-AAD-) for n = 10 animals per group. Bar graph shows the median percent of apoptosis for each group, and each point represents one animal. Statistical analysis: Kruskal-Wallis with Dunn's multiple comparison *post hoc*, * $p \leq .05$ between 5-FU and CD/OPG MSC, and ** $p \leq .01$ between PBS and 5-FU.

concentrated around the tumour area [67] and positively correlated with P-selectin expression. Moreover, although limited by animal number, we detected more engineered MSC in the tumour bearing legs than in the healthy legs in our second syngeneic model of spontaneous bone metastases. Nevertheless, future studies can further improve target specificity by exploiting irradiation of tumour sites, which is a current clinical practise for bone metastasis and known to upregulate selectins [34,64,68], other homing ligands, and chemokines. Engineering MSC with additional homing receptors (*e.g.*, HCELL [69] or CXCR4, as CXCL-12 is highly produced within the bone marrow environment [3,70,71]) could further improve their bone metastasis homing ability.

In summary, we have presented a platform technology that enables targeted delivery of biologics to disease sites, targeting multiple disease pathways in a combinatory fashion. The modularity of RNA engineering allows us to mitigate the intrinsic heterogeneity of stem cells, and to fine-tune treatments by introducing new functions to stem cells, based on patient characteristics, tumour type, and tumour stage, in a personalised way. Importantly, as MSC have been proven safe for transplantation in humans in many clinical trials, and approved for use in children with Graft-*versus*-Host disease (GvHD) [72], we anticipate that application of our system as a therapeutic could occur relatively rapidly. We will further investigate the added effect of co-delivering OPG with CD, in preserving bone integrity *in vivo,* at different stages of tumour induced bone damage. In particular, we will dissect therapeutic effects of combined *versus* monotherapies in the first intratibial model to further understand why CD/OPG MSC did not perform as potently as OPG MSC. Through our study, it became clear to us that, due to the different mechanisms of action between CD and OPG, the optimal, sustained therapeutic benefits from combinatorial treatment will likely be dependent on tumour size and bone damage levels at study entry as well as treatment schedules, which will be exploited in the future. In particular, we will assess *in vitro* and *in vivo* expression of the therapeutic factors over time for cell engineered with one or multiple factors to make sure they have comparable expression, and that there are no competition for protein translation in the case of engineering with multiple mRNA. In addition, we will further characterise the impact of monotherapies *versus* combined therapy on the bone metastatic niche, by testing sequential injection of CD MSC and OPG MSC *versus* injection of CD/OPG MSC. In particular, we would like to assess the CD's bystander effect on OPG's therapeutic function *in vivo* when killing cancer, MSC and niche cells. We remain convinced that CD and OPG co-delivered by MSC would exhibit different and complementary mechanisms in blocking the vicious circle between tumours and their niche, and therefore is advantageous in effectively managing bone metastases. Indeed, our data from the second syngeneic model, which is extremely aggressive, confirmed that combination therapy with both CD and OPG is more beneficial in treating bone metastases than monotherapies. In addition, we will characterise the amount of 5-FU converted *in vivo* by our engineered MSC and compare their tumour killing properties and associated toxicity, compared to therapeutically relevant doses of 5-FU. When moving to clinical studies, future work should systematically study the dosage, number, frequency, and schedules of treatments [73,74]. Clinical studies should also look at patient stratification based on disease stages (*e.g.* tumour sizes and bone damage levels) at study entry, in order to obtain optimal therapeutic outcome especially in the long-term. Given the profound anti-tumour effect we observed in treatments with OPG, it will be particularly interesting to investigate if our approach, of both targeting cancer cells and normalising the niche, can eradicate the metastases or at least control their growth, even with a single, transient MSC transplantation. In any case, scaling up the manufacturing process, potentially using an automated system that standardises batch-to-batch variation, and implements quality control (QC) and release assays for efficacy and toxicity, will be needed for future clinical applications [75]. Furthermore, potential immunity-mediated side effects resulting from ectopically engineered MSC should be investigated in detail.

5. Conclusions

We demonstrate a new strategy using mRNA-engineered stem cells for combinatorial targeting and delivery of multiple factors to interrogate both cancer cells and the metastatic niche in treating bone metastases. Our technology for combinatorial targeting could be extended to other types of systemic bone metastases and skeletal disorders including prostate cancer bone metastasis, multiple myeloma, and osteoporosis. As a platform technology, our system can be used to deliver other pro-dug systems [16,45], or combinations of pro-drug systems shown to be synergistic [20]. As a facile RNA delivery tool, we also envisage that our technology can be used for simultaneous delivery of next-generation genome editing components (*e.g.*, Cas9 mRNA and guide RNAs in CRISPR) [76,77] in molecular biology and gene therapy.

Supplementary data to this article can be found online at https://doi.org/10.1016/j.ebiom.2019.06.047.

Acknowledgements

We are extremely grateful to C.K.Davis for helping with animal experiments, histology and data analysis, as well as for her assistance in general experiment management. We thank F.Grun, the director of the UCI Mass Spectrometry Facility for his advice and help with the mass spectrometry analysis. We are extremely grateful to L.Zhang from the UCI ICTS BERD Unit for generating the power analysis and the linear mixed models for the *in vivo* experiments, as well as for providing general statistical consulting for the data analysis. We are very grateful to A.M.Meresse for her help with *ex vivo* experiments and tissue collection. We thank V.Pham for the flow chamber assays and his assistance with animal experiments, and we thank B.Nguyen and A.M.Ziary for their help with animal experiments, histology and DNA extraction. We thank J.Zimak and E.J.Pone for helpful discussions and comments. We thank C.W.Hughes from the Department of Cellular and Molecular Biosciences at UCI for providing the HUVEC. Servier Medical Art (www.servier.com) was used to design Fig. 1.

Funding sources

This work was supported by the NIH (1DP2CA195763-01 and R21CA219225 to W.Z.), the DOD (W81XWH-17-1-0522 to W.Z.), the contract with Baylx Inc. (BI-206512), the Fondation ARC pour la recherche sur le cancer (SAE20150602901 to A.I·S.), and the California Institute of Regenerative Medicine (EDUC2-08383 to M.T.). H.P.F. was supported by NINDS/NIH (NS082174). L.L. was supported by Baylx Inc.: BI-206512. D.L. and L.S. were supported by the National Science Foundation (NSF) under Grant CMMI-1229405. The project described was also supported by the National Center for Research Resources and the National Center for Advancing Translational Sciences, National Institutes of Health and National Cancer Institute of the National Institutes of Health under award number P30CA062203 (The content is solely the responsibility of the authors and does not necessarily represent the official views of the National Institutes of Health). The funders above did not have any involvement in the study design, data collection, data analysis, interpretation, and manuscript writing.

Author contributions

A.I·S. and W.Z. designed the research; A.I·S, J.L.C., H.P.F., M.T., C.C.Y., L.H. and L.L. performed the research; M.J.L. contributed to the *in vivo* homing study and helped with animal experiments. J.C., G.G. and M. Y·S performed the X-Ray coupled with bioluminescence imaging. D.L. and L.S. did the NanoCT imaging for the pilot study. B.T. performed the MicroCT of the main experiments on the two models. A.I.S, J.L.C., H.P.F., M.T., C.C.Y., L.H., B.T. and R.L.S. analysed and interpreted the data; A.I.S and W.Z. wrote the paper.

Declaration of Competing Interests

Dr. Segaliny reports a fellowship from Fondation ARC pour la recherche sur le cancer, grants from National Institute of Health (NIH), grants from Department Of Defense (DOD), financial support from UCI contract with Baylx Inc., grants from National Cancer Institute of the National Institutes of Health, during the conduct of the study; Mr. Farhoodi reports a T32 fellowship from National Institute of Neurological Disorders and Stroke/NIH, grants from National Institute of Health (NIH), grants from Department Of Defense (DOD), financial support from UCI contract with Baylx Inc., grants from National Cancer Institute of the National Institutes of Health, during the conduct of the study; Mr. Cheng, Mr. Yu, Mr. Toledano and Mrs. Hildebrand report grants from National Institute of Health (NIH), grants from Department Of Defense (DOD), financial support from UCI contract with Baylx Inc., grants from National Cancer Institute of the National Institutes of Health, during the conduct of the study; Dr. Linan Liu reports grants from National Institute of Health (NIH), grants from Department Of Defense (DOD), and financial support from UCI contract with Baylx Inc., during the conduct of the study. Mrs. Tierra, Mr. Liao, Mr. Liu, Dr. Sun, Dr. Cho, Dr. Gulsen, Dr. Su and Dr. Sah have nothing to disclose. Dr. Zhao reports grants from NIH, grants from DOD, financial support from Baylx Inc., non-financial support from NIH/NCI, during the conduct of the study; grants and personal fees from Baylx Inc., grants and personal fees from Velox Biosystems Inc., grants and personal fees from Amberstone Biosciences Inc., outside the submitted work.

References

[1] Mundy GR. Metastasis to bone: causes, consequences and therapeutic opportunities. Nat Rev Cancer 2002;2(8):584–93.
[2] Coleman RE. Skeletal complications of malignancy. Cancer 1997;80(8):1588–94 Suppl.
[3] Kan C, Vargas G, Pape FL, Clezardin P. Cancer cell colonisation in the bone microenvironment. Int J Mol Sci 2016;17(10).
[4] Siegel RL, Miller KD, Jemal A. Cancer statistics, 2017. CA Cancer J Clin 2017;67(1):7–30.
[5] Coleman RE. Management of bone metastases. Oncologist 2000;5(6):463–70.
[6] Coleman R, Gnant M, Morgan G, Clezardin P. Effects of bone-targeted agents on cancer progression and mortality. J Natl Cancer Inst 2012;104(14):1059–67.
[7] Petrut B, Trinkaus M, Simmons C, Clemons M. A primer of bone metastases management in breast cancer patients. Curr Oncol 2008;15(Suppl. 1):S50–7.
[8] Weilbaecher KN, Guise TA, McCauley LK. Cancer to bone: a fatal attraction. Nat Rev Cancer 2011;11(6):411–25.
[9] Mai J, Huang Y, Mu C, Zhang G, Xu R, Guo X, et al. Bone marrow endothelium-targeted therapeutics for metastatic breast cancer. J Control Release 2014;187:22–9.
[10] Saracino R, Luciano R, Battafarano G, Perrotta A, Muraca M, Del Fattore A. Nanoparticles-based treatment for bone metastasis. Curr Drug Targets 2016;17(3):303–10.
[11] Schroeder A, Heller DA, Winslow MM, Dahlman JE, Pratt GW, Langer R, et al. Treating metastatic cancer with nanotechnology. Nat Rev Cancer 2011;12(1):39–50.
[12] Swami A, Reagan MR, Basto P, Mishima Y, Kamaly N, Glavey S, et al. Engineered nanomedicine for myeloma and bone microenvironment targeting. Proc Natl Acad Sci U S A 2014;111(28):10287–92.
[13] Zhao YP, Ye WL, Liu DZ, Cui H, Cheng Y, Liu M, et al. Redox and pH dual sensitive bone targeting nanoparticles to treat breast cancer bone metastases and inhibit bone resorption. Nanoscale 2017;9(19):6264–77.
[14] Wilhelm S, Tavares AJ, Dai Q, Ohta S, Audet J, Dvorak HF, et al. Analysis of nanoparticle delivery to tumours. Nat Rev Mater 2016;1(5).
[15] Droujinine IA, Eckert MA, Zhao W. To grab the stroma by the horns: from biology to cancer therapy with mesenchymal stem cells. Oncotarget 2013;4(5):651–64.
[16] Shah K. Mesenchymal stem cells engineered for cancer therapy. Adv Drug Deliv Rev 2012;64(8):739–48.
[17] Du WL, Seah I, Bougazzoul O, Choi GH, Meeth K, Bosenberg MW, et al. Stem cell-released oncolytic herpes simplex virus has therapeutic efficacy in brain metastatic melanomas. Proc Natl Acad Sci USA 2017;114(30):E6157–65.
[18] Grisendi G, Bussolari R, Cafarelli L, Petak I, Rasini V, Veronesi E, et al. Adipose-derived mesenchymal stem cells as stable source of tumor necrosis factor-related apoptosis-inducing ligand delivery for Cancer therapy. Cancer Res 2010;70(9):3718–29.
[19] Liu LN, Zhang SX, Liao WB, Farhoodi HP, Wong CW, Chen CC, et al. Mechanoresponsive stem cells to target cancer metastases through biophysical cues. Sci Transl Med 2017;9(400).
[20] Matuskova M, Kozovska Z, Toro L, Durinikova E, Tyciakova S, Cierna Z, et al. Combined enzyme/prodrug treatment by genetically engineered AT-MSC exerts synergy and inhibits growth of MDA-MB-231 induced lung metastases. J Exp Clin Cancer Res 2015;34.
[21] Studeny M, Marini FC, Champlin RE, Zompetta C, Fidler IJ, Andreeff M. Bone marrow-derived mesenchymal stem cells as vehicles for interferon-beta delivery into tumors. Cancer Res 2002;62(13):3603–8.
[22] Yi BR, Hwang KA, Aboody KS, Jeung EB, Kim SU, Choi KC. Selective antitumor effect of neural stem cells expressing cytosine deaminase and interferon-beta against ductal breast cancer cells in cellular and xenograft models. Stem Cell Res 2014;12(1):36–48.
[23] Niess H, von Einem JC, Thomas MN, Michl M, Angele MK, Huss R, et al. Treatment of advanced gastrointestinal tumors with genetically modified autologous mesenchymal stromal cells (TREAT-ME1): study protocol of a phase I/II clinical trial. BMC Cancer 2015;15:237.
[24] Schweitzer KM, Drager AM, van der Valk P, Thijsen SF, Zevenbergen A, Theijsmeijer AP, et al. Constitutive expression of E-selectin and vascular cell adhesion molecule-1 on endothelial cells of hematopoietic tissues. Am J Pathol 1996;148(1):165–75.
[25] Sipkins DA, Wei X, Wu JW, Runnels JM, Cote D, Means TK, et al. In vivo imaging of specialized bone marrow endothelial microdomains for tumour engraftment. Nature 2005;435(7044):969–73.
[26] Xia L, McDaniel JM, Yago T, Doeden A, McEver RP. Surface fucosylation of human cord blood cells augments binding to P-selectin and E-selectin and enhances engraftment in bone marrow. Blood 2004;104(10):3091–6.
[27] Nouri FS, Wang X, Hatefi A. Genetically engineered theranostic mesenchymal stem cells for the evaluation of the anticancer efficacy of enzyme/prodrug systems. J Control Release 2015;200:179–87.
[28] Body JJ, Greipp P, Coleman RE, Facon T, Geurs F, Fermand JP, et al. A phase I study of AMGN-0007, a recombinant osteoprotegerin construct, in patients with multiple myeloma or breast carcinoma related bone metastases. Cancer 2003;97(3 Suppl):887–92.
[29] Higgs JT, Jarboe JS, Lee JH, Chanda D, Lee CM, Deivanayagam C, et al. Variants of osteoprotegerin lacking TRAIL binding for therapeutic bone remodeling in osteolytic malignancies. Mol Cancer Res 2015;13(5):819–27.
[30] NguyenThai QA, Sharma N, Luong do H, Sodhi SS, Kim JH, Kim N, et al. Targeted inhibition of osteosarcoma tumor growth by bone marrow-derived mesenchymal stem cells expressing cytosine deaminase/5-fluorocytosine in tumor-bearing mice. J Gene Med 2015;17(3–5):87–99.
[31] Qiao B, Shui W, Cai L, Guo SQ, Jiang DM. Human mesenchymal stem cells as delivery of osteoprotegerin gene: homing and therapeutic effect for osteosarcoma. Drug Des Dev Ther 2015;9:969–76.
[32] Kariko K, Muramatsu H, Welsh FA, Ludwig J, Kato H, Akira S, et al. Incorporation of pseudouridine into mRNA yields superior nonimmunogenic vector with increased translational capacity and biological stability. Mol Ther 2008;16(11):1833–40.
[33] Lee J, Dykstra B, Spencer JA, Kenney LL, Greiner DL, Shultz LD, et al. mRNA-mediated glycoengineering ameliorates deficient homing of human stem cell-derived hematopoietic progenitors. J Clin Invest 2017;127(6):2433–7.
[34] Levy O, Zhao WA, Mortensen LJ, LeBlanc S, Tsang K, Fu MY, et al. mRNA-engineered mesenchymal stem cells for targeted delivery of interleukin-10 to sites of inflammation. Blood 2013;122(14):E23–32.
[35] Sekiya I, Larson BL, Smith JR, Pochampally R, Cui JG, Prockop DJ. Expansion of human adult stem cells from bone marrow stroma: conditions that maximize the yields of early progenitors and evaluate their quality. Stem Cells 2002;20(6):530–41.
[36] Dominici M, Le Blanc K, Mueller I, Slaper-Cortenbach I, Marini FC, Krause DS, et al. Minimal criteria for defining multipotent mesenchymal stromal cells. The International Society for Cellular Therapy position statement. Cytotherapy 2006;8(4):315–7.
[37] Kuchimaru T, Kataoka N, Nakagawa K, Isozaki T, Miyabara H, Minegishi M, et al. A reliable murine model of bone metastasis by injecting cancer cells through caudal arteries. Nat Commun 2018;9.
[38] Swain SM, Lippman ME, Egan EF, Drake JC, Steinberg SM, Allegra CJ. Fluorouracil and high-dose leucovorin in previously treated patients with metastatic breast-Cancer. J Clin Oncol 1989;7(7):890–9.
[39] Schneider T, Osl F, Friess T, Stockinger H, Scheuer WV. Quantification of human Alu sequences by real-time PCR–an improved method to measure therapeutic efficacy of anti-metastatic drugs in human xenotransplants. Clin Exp Metastasis 2002;19(7):571–82.
[40] Yasuma T, Yano Y, D'Alessandro-Gabazza CN, Toda M, Gil-Bernabe P, Kobayashi T, et al. Erratum. Amelioration of Diabetes by Protein S. Diabetes 2016;65:1940–51 (Diabetes. 2016;65(12):3812).
[41] McBride C, Gaupp D, Phinney DG. Quantifying levels of transplanted murine and human mesenchymal stem cells in vivo by real-time PCR. Cytotherapy 2003;5(1):7–18.
[42] Funakoshi K, Bagheri M, Zhou M, Suzuki R, Abe H, Akashi H. Highly sensitive and specific Alu-based quantification of human cells among rodent cells. Sci Rep-UK 2017;7.
[43] Ley K, Laudanna C, Cybulsky MI, Nourshargh S. Getting to the site of inflammation: the leukocyte adhesion cascade updated. Nat Rev Immunol 2007;7(9):678–89.
[44] Baud'huin M, Duplomb L, Teletchea S, Lamoureux F, Ruiz-Velasco C, Maillasson M, et al. Osteoprotegerin: multiple partners for multiple functions. Cytokine Growth Factor Rev 2013;24(5):401–9.
[45] Kucerova L, Durinikova E, Toro L, Cihova M, Miklikova S, Poturnajova M, et al. Targeted antitumor therapy mediated by prodrug-activating mesenchymal stromal cells. Cancer Lett 2017;408:1–9.
[46] Aboody KS, Najbauer J, Schmidt NO, Yang W, Wu JK, Zhuge Y, et al. Targeting of melanoma brain metastases using engineered neural stem/progenitor cells. Neuro-Oncology 2006;8(2):119–26.
[47] Cameron DA, Gabra H, Leonard RC. Continuous 5-fluorouracil in the treatment of breast cancer. Br J Cancer 1994;70(1):120–4.
[48] Winkler IG, Barbier V, Nowlan B, Jacobsen RN, Forristal CE, Patton JT, et al. Vascular niche E-selectin regulates hematopoietic stem cell dormancy, self renewal and chemoresistance. Nat Med 2012;18(11):1651–7.

[49] Stubke K, Wicklein D, Herich L, Schumacher U, Nehmann N. Selectin-deficiency reduces the number of spontaneous metastases in a xenograft model of human breast cancer. Cancer Lett 2012;321(1):89–99.
[50] Wright LE, Ottewell PD, Rucci N, Peyruchaud O, Pagnotti GM, Chiechi A, et al. Murine models of breast cancer bone metastasis. Bonekey Rep 2016;5.
[51] Andersen C, Bagi CM, Adams SW. Intra-tibial injection of human prostate cancer cell line CWR22 elicits osteoblastic response in immunodeficient rats. J Musculoskelet Neuronal Interact 2003;3(2):148–55.
[52] Karp JM, Teol GSL. Mesenchymal stem cell homing: the devil is in the details. Cell Stem Cell 2009;4(3):206–16.
[53] Wang H, Cao F, De A, Cao Y, Contag C, Gambhir SS, et al. Trafficking mesenchymal stem cell engraftment and differentiation in tumor-bearing mice by bioluminescence imaging. Stem Cells 2009;27(7):1548–58.
[54] Direcks WGE, van Gelder M, Lammertsma AA, Molthoff CFM. A new rat model of human breast cancer for evaluating efficacy of new anti-cancer agents in vivo. Cancer Biol Ther 2008;7(4):532–7.
[55] Shaikh A, Bhartiya D, Kapoor S, Nimkar H. Delineating the effects of 5-fluorouracil and follicle-stimulating hormone on mouse bone marrow stem/progenitor cells. Stem Cell Res Ther 2016;7(1):59.
[56] Hiraga T, Ueda A, Tamura D, Hata K, Ikeda F, Williams PJ, et al. Effects of oral UFT combined with or without zoledronic acid on bone metastasis in the 4T1/luc mouse breast cancer. Int J Cancer 2003;106(6):973–9.
[57] Michailidou M, Holen I. Combinations of bisphosphonates and classical anticancer drugs: a preclinical perspective. Recent Results Cancer Res 2012;192:145–69.
[58] Ottewell PD, Wang N, Brown HK, Fowles CA, Croucher PI, Eaton CL, et al. OPG-fc inhibits ovariectomy-induced growth of disseminated breast cancer cells in bone. Int J Cancer 2015;137(4):968–77.
[59] Nowakowski A, Andrzejewska A, Janowski M, Walczak P, Lukomska B. Genetic engineering of stem cells for enhanced therapy. Acta Neurobiol Exp 2013;73(1):1–18.
[60] Thomas CE, Ehrhardt A, Kay MA. Progress and problems with the use of viral vectors for gene therapy. Nat Rev Genet 2003;4(5):346–58.
[61] Devine SM, Bartholomew AM, Mahmud N, Nelson M, Patil S, Hardy W, et al. Mesenchymal stem cells are capable of homing to the bone marrow of non-human primates following systemic infusion. Exp Hematol 2001;29(2):244–55.
[62] Kidd S, Spaeth E, Dembinski JL, Dietrich M, Watson K, Klopp A, et al. Direct evidence of mesenchymal stem cell tropism for tumor and wounding microenvironments using in vivo bioluminescent imaging. Stem Cells 2009;27(10):2614–23.
[63] Jackson W, Sosnoski DM, Ohanessian SE, Chandler P, Mobley A, Meisel KD, et al. Role of megakaryocytes in breast Cancer metastasis to bone. Cancer Res 2017;77(8):1942–54.
[64] Shamay Y, Elkabets M, Li HY, Shah J, Brook S, Wang F, et al. P-selectin is a nanotherapeutic delivery target in the tumor microenvironment. Sci Transl Med 2016;8(345).
[65] Suva LJ, Washam C, Nicholas RW, Griffin RJ. Bone metastasis: mechanisms and therapeutic opportunities. Nat Rev Endocrinol 2011;7(4):208–18.
[66] Zhao WA, Loh W, Droujinine IA, Teo WS, Kumar N, Schafer S, et al. Mimicking the inflammatory cell adhesion cascade by nucleic acid aptamer programmed cell-cell interactions. FASEB J 2011;25(9):3045–56.
[67] Lorincz T, Timar J, Szendroi M. Alterations of microvascular density in bone metastases of adenocarcinomas. Pathol Oncol Res 2004;10(3):149–53.
[68] Klopp AH, Spaeth EL, Dembinski JL, Woodward WA, Munshi A, Meyn RE, et al. Tumor irradiation increases the recruitment of circulating mesenchymal stem cells into the tumor microenvironment. Cancer Res 2007;67(24):11687–95.
[69] Sackstein R, Merzaban JS, Cain DW, Dagia NM, Spencer JA, Lin CP, et al. Ex vivo glycan engineering of CD44 programs human multipotent mesenchymal stromal cell trafficking to bone. Nat Med 2008;14(2):181–7.
[70] Bobis-Wozowicz S, Miekus K, Wybieralska E, Jarocha D, Zawisz A, Madeja Z, et al. Genetically modified adipose tissue-derived mesenchymal stem cells overexpressing CXCR4 display increased motility, invasiveness, and homing to bone marrow of NOD/SCID mice. Exp Hematol 2011;39(6):686–696 e684.
[71] Wynn RF, Hart CA, Corradi-Perini C, O'Neill L, Evans CA, Wraith JE, et al. A small proportion of mesenchymal stem cells strongly expresses functionally active CXCR4 receptor capable of promoting migration to bone marrow. Blood 2004;104(9):2643–5.
[72] LeBlanc K, Frassoni F, Ball L, Locatelli F, Roelofs H, Lewis I, et al. Mesenchymal stem cells for treatment of steroid-resistant, severe, acute graft-versus-host disease: a phase II study. Lancet 2008;371(9624):1579–86.
[73] Jarocha D, Milczarek O, Wedrychowicz A, Kwiatkowski S, Majka M. Continuous improvement after multiple mesenchymal stem cell transplantations in a patient with complete spinal cord injury. Cell Transplant 2015;24(4):661–72.
[74] Kucerova L, Skolekova S, Demkova L, Bohovic R, Matuskova M. Long-term efficiency of mesenchymal stromal cell-mediated CD-MSC/5FC therapy in human melanoma xenograft model. Gene Ther 2014;21(10):874–87.
[75] Special issue on Cell Therapy Manufacturing and Scale-Up Introduction: TA Brieva, Celgene. Scale-up and manufacturing of cell-based therapies IV. Biochem Eng J 2016;108:1–2.
[76] Bak RO, Hendel A, Clark JT, Kennedy AB, Ryan DE, Roy S, et al. Chemically modified guide RNAs enhance CRISPR/Cas genome editing in human primary cells. Hum Gene Ther 2015;26(10):A11–2.
[77] Chen ZH, Yu YP, Zuo ZH, Nelson JB, Michalopoulos GK, Monga S, et al. Targeting genomic rearrangements in tumor cells through Cas9-mediated insertion of a suicide gene. Nat Biotechnol 2017;35(6):543.